## NOTICE

**The quality of this microform is heavily dependent upon the quality of the original thesis submitted for microfilming. Every effort has been made to ensure the highest quality of reproduction possible.**

**If pages are missing, contact the university which granted the degree.**

**Some pages may have indistinct print especially if the original pages were typed with a poor typewriter ribbon or if the university sent us an inferior photocopy.**

**Reproduction in full or in part of this microform is governed by the Canadian Copyright Act, R.S.C. 1970, c. C-30, and subsequent amendments.**

## AVIS

**La qualité de cette microforme dépend grandement de la qualité de la thèse soumise au microfilmage. Nous avons tout fait pour assurer une qualité supérieure de reproduction.**

**S'il manque des pages, veuillez communiquer avec l'université qui a conféré le grade.**

**La qualité d'impression de certaines pages peut laisser à désirer, surtout si les pages originales ont été dactylographiées à l'aide d'un ruban usé ou si l'université nous a fait parvenir une photocopie de qualité inférieure.**

**La reproduction, même partielle, de cette microforme est soumise à la Loi canadienne sur le droit d'auteur, SRC 1970, c. C-30, et ses amendements subséquents.**

Canada

# SURFACE MAGNETO-OPTICAL KERR EFFECT FOR ULTRATHIN NI-FE BILAYERS

by

Qingming Zhong
B.Sc.(Nuclear Electronics), University
of Science and Technology of China, 1982
M. Sc. USTC, 1986

A THESIS SUBMITTED IN PARTIAL FULFILLMENT OF
THE REQUIRMENTS FOR THE DEGREE OF
MASTER OF SCIENCE
in the Department
of
Physics



SIMON FRASER UNIVERSITY
JUNE 1991

ISBN 0-315-78168-8

## APPROVAL

Name: Qingming Zhong

Degree: Master of Science

Title of Thesis: Surface Magneto-optical Kerr Effect for Ultrathin Ni-Fe Bilayers.

Examining Committee:

Dr. K. E. Rieckhoff, Chairman

Dr. A. S. Arrott
Senior Supervisor

Dr. B. Heinrich
Supervisor

Dr. L. H. Palmer

Dr. J. F. Cochran, Examiner

Date of Approval: July 22, 1991

## PARTIAL COPYRIGHT LICENSE

I hereby grant to Simon Fraser University the right to lend my thesis, project or extended essay (the title of which is shown below) to users of the Simon Fraser University Library, and to make partial or single copies only for such users or in response to a request from the library of any other university, or other educational institution, on its own behalf or for one of its users. I further agree that permission for multiple copying of this work for scholarly purposes may be granted by me or the Dean of Graduate Studies. It is understood that copying or publication of this work for financial gain shall not be allowed without my written permission.

Title of Thesis/Project/Extended Essay

**Surface Magneto-Optical Kerr Effect for Ultrathin Ni-Fe Bilayers**

Author: _____
(Signature)

Qing-ming Zhong
(Name)

July 11, 1991
(Date)

## ABSTRACT

Surface magneto-optical Kerr effect is used to measure magnetic hysteresis loops for Ni/Fe bilayers previously studied by ferromagnetic resonance [Phys. Rev. B. 38, 12879 (1988)]. The approach to saturation along sample's hard axis confirms the existence of an enhanced fourfold inplane magnetic anisotropy. The effect is attributed to arrays of misfit dislocations arising from a reconstruction that occurs during the epitaxial growth of Ni overlayers on ultrathin layers of bcc (001) Fe. The [11] magnetization curves for 10 monolayers of Ni on 7 monolayers of Fe shows an asymmetry with respect to field direction. The polar Kerr effect experiment confirms that this broken symmetry appears with the nucleation of domains during magnetization. It might be because some spin configurations freeze during growth which have the magnetization component out of the plane in one direction.

We also investigate coercivity at lower temperatures for several Ni/Fe bilayer samples. Experiments show that the unreconstructed bcc Ni overlayers have very little effect on the magnetic properties of ultrathin Fe on Ag. The reconstructed Ni overlayers increase the coercivity about 30 times.

## Acknowledgements

It has been a great honor and privilege for me to have been supervised by Dr. Anthony S. Arrott during the course of this research. I gratefully acknowledge his guidance and assistance of my work.

I also wish to thank our laboratory director Dr. B. Heinrich for valuable discussions and his help to my experiments.

The work reported in this thesis in very much the result of a collaborative effort by our research group. I wish to thank Z. Celinski for sample preparation. I really appreciate all the help I received from Stephen T. Purcell, Ken Myrtle, Jeff Rudd and other members in our group.

## TABLE OF CONTENTS


Approval ____ ii

Abstract ____ iii

Acknowledgements ____ iv

Table of Contents ____ v

List of Figures ____ vii

**1. Introduction** ____ 1

**2. Theory of Magneto-optical Kerr Effects** ____ 5

2.1 Introduction ____ 5

2.2 Phenomenological Model of Kerr Effects ____ 6

2.3 Fresnel Reflection Coefficient ____ 12

2.4 Experimental Signals ____ 17

2.5 Discussion ____ 21

2.6 References ____ 23

**3. Experimental Apparatus** ____ 24

3.1 Magneto-optical Kerr Effect System ____ 24

3.2 Experiment Setup and Procedures ____ 33

3.3 Sample Preparation ____ 34

3.4 References ____ 36

**4. Experimental Results and Discussions** ____ 38

4.1 Introduction ____ 38

4.2 Sample Description ____ 39

4.3 Hysteresis Loops of Ni/Fe Bilayers ____ 41
4.4 Coercivity as a Function of Temperature ____ 48
4.5 Discussion ____ 50
4.6 Conclusions ____ 52
4.7 References ____ 53

**5. List of Appendices** ____ 55
Appendix 1: Kerr Effect Data Processing Program ____ 56
Appendix 2: Data Measurement Procedures ____ 64
Appendix 3: Temperature Control Program ____ 67

## LIST OF FIGURES


Fig.2.1 _____ 5

Fig.2.2 _____ 17

Fig.2.3 _____ 22

Fig.3.1 _____ 25

Fig.3.2 _____ 26

Fig.3.3 _____ 28

Fig.3.4 _____ 30

Fig.3.5 _____ 32

Fig.3.6 _____ 34

Fig.3.7 _____ 35

Fig.4.1 _____ 42

Fig.4.2 _____ 44

Fig.4.3 _____ 45

Fig.4.4 _____ 46

Fig.4.5 _____ 47

Fig.4.6 _____ 49

Fig.4.7 _____ 51

# Chapter 1

## Introduction

In this thesis we describe surface magneto-optical Kerr effect studies of the magnetic properties of ultrathin epitaxial Ni/Fe bilayers on Ag (001). The study of Ni/Fe bilayers on Ag (001) was started two years ago in our surface physics laboratory. We use molecular beam epitaxy (MBE) techniques to grow an ultrathin Ni/Fe bilayer on a Ag single crystal substrate. By using ferromagnetic resonance (FMR), reflection high energy electron diffraction (RHEED), X-ray photoelectron spectroscopy (XPS) and Auger electron spectroscopy techniques, previous studies showed that bcc Ni overlayers can be epitaxially grown on ultrathin Fe films that were grown on the Ag (001) single crystal. The Ni overlayers have a critical thickness, about three to five monolayers, for lattice reconstruction. The experimental results show that the unreconstructed Ni overlayers had only small effects on the Fe FMR signals. But reconstructed Ni overlayers created a large four-fold in-plane magnetic anisotropy with the easy axis along the Fe [100] crystallographic direction. The anisotropy was ten to twenty times larger than bulk fcc Ni.

Previously FMR studies of Ni/Fe bilayers obtained most of their results from data in external magnetic fields sufficient to saturate the magnetization. In order to more fully understand the structural and magnetic properties of the Ni/Fe bilayers, we had to

investigate their behavior in magnetic fields below saturation. The surface magneto-optical Kerr effect is a valuable method for this purpose. Information about the structural order of the reflecting layer might be obtained from the light itself. Levkov [1.1] has shown that the existence or absence of the Kerr effect in the surface of ferromagnetic metal directly indicates not only the existence of a crystalline structure in the surface layer, but also the order of this structure. The Kerr effect technique has been used by many researchers in the study of magnetic thin films.[1.2-1.6]

In order to prevent oxidation of the thin film surface, our Ni/Fe bilayers are all covered with 20 to 30 monolayers of Au. The He-Ne laser beam can easily penetrate these Au overlayers.

Chapter two contains descriptions of magneto-optical Kerr effect theory. By using a phenomenological model, the Kerr effect is described by the permittivity tensor with off diagonal elements. These elements depend upon the Voigt magneto-optical parameter Q which is a function of magnetization M. There are three kinds of Kerr effects (polar, longitudinal and transverse) based on the fact that the magnitude and sign of the rotation of the plane polarized reflected light depends on the magnitude and direction of the surface magnetization.

The theory shows that our experimental system can be made sensitive to only the polar and longitudinal Kerr effects. Usually, we observe the combined signals from the polar and longitudinal

Kerr effects. By letting the angle of incidence approach to zero, we can easily distinguish between these two kinds of Kerr effect.

Chapter 3 describes our experimental system and the operating procedures. In Chapter 4 the results from several Ni/Fe bilayer samples are given. The [11] magnetization curves for Ni/Fe(10/6.6) and Ni/Fe(10/7) shows a breaking of symmetry between positive and negative field. This interesting phenomena may be caused by spin configuration frozen during growth. Our results agree with former studies from FMR that the unreconstructed Ni overlayers have no effect on the magnetic properties of ultrathin Fe on Ag (001) substrate. Low temperature study of coercive force behavior also has been carried out in this thesis. Detailed discussion can found in Chapter 4.

## 1.2 References

[1.1] Sokolov "Optical Properties of Metals".

[1.2]C. Liu, S. D. Bader, "Surface Magneto-optical Studies of Ultrathin Ferromagnetic Films", Material Division, Argonne National Laboratory, May, 1989.

[1.3] D. H. Martin, K. F. Neal and T. J. Dean, "The Optical and Magneto-optical Behaviour of Ferromagnetic Metals", Proc. Phys. Soc., 1965, Vol. 86.

[1.4] E. R. Moog and S. D. Bader, "Magneto-optical Studies of Ultra-thin Epitaxial Films of fcc Fe on Cu(100)", IEEE Transaction on Magnetics, Vol. MAG-23, No. 5, Sept., 1987.

[1.5] P. Q. J. Nederpel and J. W. D. Martens, "Magneto-optical Ellipsometer". Rev. Sci. Instrum. 56(5), May, 1985.

[1.6] J. M. Florczak and E. Dan Dahlberg, "Detecting Two Magnetization Components by The Magneto-optical Kerr Effect". To be published.

# Chapter 2.

# Theory of Magneto-Optical Kerr Effects

## 2.1 Introduction

The magneto-optical Kerr effects are categorized according to the geometry of the magnetization in relation to the plane of incidence and the film plane. In the polar Kerr effect, the magnetization is perpendicular to the surface of the sample and parallel to the plane of incidence. In the longitudinal Kerr effect, the magnetization is parallel both to the surface of sample and the incident plane. In the case of transverse Kerr effect, the magnetization is parallel to the sample surface but perpendicular to the incident plane. See Fig. 2.1

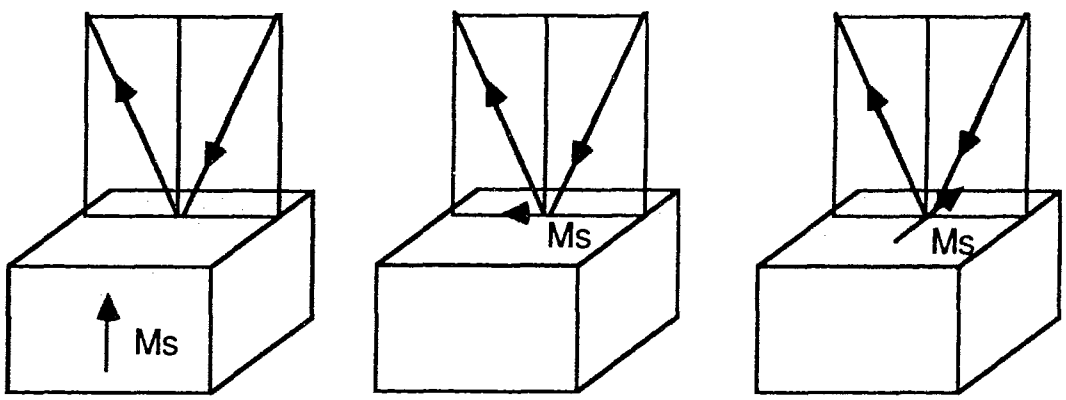


Fig.2.1

In discussing the polarization of light we refer to the electric field E, not the magnetic field H. Thus if a wave is described as

linearly polarized along the x direction, it is E that is vibrating along the x axis, not H.

If the magnetization vector is oriented as one of the cases in Fig. 2.1, then in addition to the linear oscillations of electrons in the metal due to the electric vector of the incident light, there is also an oscillation at right angles to this direction, owing to the Lorentz force. Accordingly, the reflected light includes a perpendicular component, known as the Kerr component. This means that the reflected light is in fact elliptically polarized (in the absence of magnetization it should be plane polarized). In the case of longitudinal magnetization and normal incidence there is no Kerr effect. The Kerr effect only appears at oblique incidence. In the case of transverse magnetization the symmetry properties again exclude a special effect if the electric vector in the incident light is parallel or perpendicular to the incidence plane.

## 2.2 Phenomenological Model of Kerr Effects

In the phenomenological model,[2.1-2.4] the Kerr effect is described by the permittivity tensor with off-diagonal elements. These elements depend upon the Voigt magneto-optical parameter Q. Residing in this parameter is the interaction of the electromagnetic field with the magnetic electrons. By virtue of this, Q is proportional to the magnetization in the ferromagnet.

For anisotropic materials, the permittivity tensor is

$$\varepsilon' = \begin{pmatrix} \varepsilon'_{xx} & \varepsilon'_{xy} & \varepsilon'_{xz} \\ \varepsilon'_{xy} & \varepsilon'_{yy} & \varepsilon'_{yz} \\ \varepsilon'_{xz} & \varepsilon'_{yz} & \varepsilon'_{zz} \end{pmatrix} + i \begin{pmatrix} 0 & -\varepsilon''_{xy} & \varepsilon''_{xz} \\ \varepsilon''_{xy} & 0 & -\varepsilon''_{yz} \\ -\varepsilon''_{xz} & \varepsilon''_{yz} & 0 \end{pmatrix} \qquad (1)$$

even in **M** odd in **M**

Without loss of generality, we suppose that the magnetization vector M is in the z-direction. So we have

$\varepsilon'_{xz} = \varepsilon'_{yz} = \varepsilon''_{xz} = \varepsilon''_{yz} = 0$. $\varepsilon'_{xx} = \varepsilon'_{yy} = \varepsilon'$ and $\varepsilon'_{zz} = \varepsilon'_o = (\mathbf{n}\text{-}ik)^2 = n^2$

Where **n** is the principal refractive index and k is the principal absorption coefficient. We can rewrite the tensor [2.6(p389)]

$$\varepsilon' = \begin{pmatrix} \varepsilon' & -i\varepsilon' Q & 0 \\ i\varepsilon' Q & \varepsilon' & 0 \\ 0 & 0 & \varepsilon'_o \end{pmatrix} \qquad (2)$$

$$\text{where } Q = \frac{4\pi}{i\varepsilon'_o}\left(\alpha_1 + \frac{\sigma_1}{i\omega}\right) = Q_o + iQ'$$

$\alpha_1$ and $\sigma_1$ are the elements of the polarizability and the conductivity tensors. In quantum theory they are[2.5]

$$\alpha_1 = \frac{2\pi ec}{m\omega^2}\left[\sum_{m>n}(Q_{mn}\delta(\omega_{mn} - \omega))av\right]M, \quad |\alpha_1| = \begin{cases} 4.0\times10^{-3} \text{ for Fe} \\ 1.6\times10^{-3} \text{ for Ni} \end{cases} \qquad (3)$$

$$\sigma_1 = -\frac{4ec}{m}\left[\sum_{m>n}\left(\frac{Q_{mn}}{\omega^2_{mn} - \omega^2}\right)av\right]M, \quad |\sigma_1| = \begin{cases} 12.4\times10^{12}\text{sec}^{-1} \text{ for Fe} \\ 5.2\times10^{12}\text{sec}^{-1} \text{ for Ni} \end{cases} \qquad (4)$$

The numbers in brackets are measured for $h\omega/2\pi = 3.0\times10^{-12}$ erg, $\lambda = 6000$Å. $M \approx 500$ Gauss for Ni, under saturation conditions at room temperature. $M \approx 1715$ Gauss for Fe, under saturation condition at room temperature.[2.5] $M = M_s\beta_3$ is the magnetization average over the sampled area. $\beta_3$ is the mean value of the direction cosine of the resultant spin relative to the z-axis.

The diagonal components of the permittivity tensor $\varepsilon'_{xx}$ and $\varepsilon'_{yy}$ are also function of the magneto-optical parameter Q. Experiment shows that this Q is very small ($Q << 1$) and therefore the function $\varepsilon'(Q)$ may be expanded into a series in increasing power of Q. The first three terms are often sufficient, i.e.[2.5]

$$\varepsilon'(Q) = \varepsilon'_o + \left(\frac{\delta\varepsilon'}{\delta Q}\right)_{Q=0} Q + \frac{1}{2}\left(\frac{\delta^2\varepsilon'}{\delta Q^2}\right)_{Q=0} Q^2 \qquad (5)$$

When the direction of the magnetization vector is reversed, the latter expression becomes

$$\varepsilon'(-Q) = \varepsilon'_o - \left(\frac{\delta\varepsilon'}{\delta Q}\right)_{Q=0} Q + \frac{1}{2}\left(\frac{\delta^2\varepsilon'}{\delta Q^2}\right)_{Q=0} Q^2 \qquad (6)$$

Moreover, $\varepsilon'(-Q) = \varepsilon'(Q)$, since $D = \varepsilon' E$ must be invariant under magnetization reversal. We must have

$$\varepsilon'(Q) = \varepsilon'_o + \frac{1}{2}\left(\frac{\delta^2\varepsilon'}{\delta Q^2}\right)_{Q=0} Q^2 = \varepsilon'_o + \varepsilon'_o f Q^2, \text{ where } f = \frac{1}{2\varepsilon'_o}\left(\frac{\delta^2\varepsilon'}{\delta Q^2}\right)_{Q=0}$$

We see that as $\varepsilon'(Q)$ is even in Q, it has no contribution to the Kerr effect. If we ignore the $Q^2$ term, we will have that $\varepsilon' = \varepsilon'_o$.

Let us rewrite the permittivity tensor

$$\varepsilon' = \begin{pmatrix} \varepsilon'_o & -i\varepsilon'_o Q & 0 \\ i\varepsilon'_o Q & \varepsilon'_o & 0 \\ 0 & 0 & \varepsilon'_o \end{pmatrix} \qquad (7)$$

for **M** parallel to z-axis.

The off diagonal components of the permittivity tensor are proportional to the resultant magnetization. This Q gives all the magneto-optical Kerr effects.

Let us consider a plane homogeneous wave in a ferromagnetic metal film. According to Maxwell's equations in the metal, we have

$$\frac{1}{c}\frac{\partial D}{\partial t} = \text{curl } H, \qquad (8)$$

$B = \mu H$, $\mu \approx 1$ in the visible range even for ferromagnetism.

$$\frac{1}{c}\frac{\partial B}{\partial t} = -\text{curl } E, \qquad D = \varepsilon' E \qquad (9)$$

$$\text{div } E = 0, \qquad \text{inside the sample}$$

$$\text{div } B = 0.$$

For a plane wave in the medium, we write

$$E = E_o e^{-i\omega t + i\frac{(\alpha x + \beta y + \gamma z)}{v}} \qquad (10)$$

where $v = \frac{V}{1 - i\chi}$ is the complex velocity. V is the real velocity. $\chi$ is a quantity related to the absorption coefficient ($\chi n = k$) and $\alpha, \beta, \gamma$ are complex numbers, where real parts $\alpha', \beta', \gamma'$ are the direction cosines of the wave normal. It will be necessary in our subsequent analysis to use inhomogeneous waves whose amplitudes vary over the wave front and for which the planes of the equal phases are at an angle to the plane of equal amplititudes, the angle being the real angle of refraction. The phase of such wave can be written in the form [2.6]

$$\omega\left(t - \frac{\alpha' x + \beta' y + \gamma' z - i\chi(\alpha'' x + \beta'' y + \gamma'' z)}{V}\right) \qquad (11)$$

Where $\alpha', \beta' \gamma'$ are the direction cosines of the normal to the plane of equal phases and $\alpha'', \beta'', \gamma''$ are the direction cosines of the normal to the plane of equal amplititudes. If we use the substitutions

$$(\alpha' - i\chi\alpha'')^2 + (\beta' - i\chi\beta'')^2 + (\gamma' - i\chi\gamma'')^2$$
$$= 1 - \chi^2 - i2\chi(\alpha'\alpha'' + \beta'\beta'' + \gamma'\gamma'') = R^2 \qquad (12)$$

$$\alpha^* = \frac{\alpha' - i\chi\alpha''}{R}, \quad \beta^* = \frac{\beta' - i\chi\beta''}{R}, \quad \gamma^* = \frac{\gamma' - i\chi\gamma''}{R}, \quad v^* = \frac{V}{R}$$

$\alpha^{*2} + \beta^{*2} + \gamma^{*2} = 1$ we have

$$E = E_o e^{-i\omega t + i\omega \frac{\alpha^* x + \beta^* y + \gamma^* z}{v^*}} \qquad (13)$$

If we take the curl of equation (8) and use (9), we find

$$c^2(\Delta E - \text{grad div}E) = \frac{\partial^2 D}{\partial t^2} \qquad (14)$$

Substituting $D = \varepsilon' E$ into (14), we have

$$\begin{cases} c^2(\Delta E_x - \text{grad}_x \text{div}E) = \varepsilon'_o \ddot{E}_x - i\varepsilon'_o Q \ddot{E}_y \\ c^2(\Delta E_y - \text{grad}_y \text{div}E) = \varepsilon'_o \ddot{E}_y + i\varepsilon'_o Q \ddot{E}_x \\ c^2(\Delta E_z - \text{grad}_z \text{div}E) = \varepsilon'_o \ddot{E}_z \end{cases} \qquad (15)$$

$$\begin{cases} \varepsilon'_o E_x - i\varepsilon'_o Q E_y = n^{*2}[E_x - \alpha^*(\alpha^* E_x + \beta^* E_y + \gamma^* E_z)] \\ \varepsilon'_o E_y + i\varepsilon'_o Q E_x = n^{*2}[E_y - \beta^*(\alpha^* E_x + \beta^* E_y + \gamma^* E_z)] \\ \varepsilon'_o E_z = n^{*2}[E_z - \gamma^*(\alpha^* E_x + \beta^* E_y + \gamma^* E_z)] \end{cases} \qquad (16)$$

where $n^* = c/v^*$ is the complex refractive index of the magnetized ferromagnetic. For the homogeneous equation, the determinant must vanish. We can eliminate $E_x$, $E_y$ and $E_z$ in (16) and obtain the following equation for $n^*$:

$$n^* - \{\varepsilon'_o(1 - Q^2)(\alpha^* + \beta^*) + \varepsilon'_o(1 + \gamma^*)\}n^{*2} + \varepsilon_o'^2(1 - Q^2) = 0. \qquad (17)$$

Solving for $n^*$ and dropping terms of the order of $Q^2$, we get

$$n^{*2}_{\pm} = \varepsilon'_o(1 \pm \gamma^* Q) + \frac{\varepsilon'_o Q^2(1 - \gamma^{*2})}{2} + \ldots . \qquad (18)$$

$$n^*_{\pm} \approx n(1 \pm \frac{\gamma^* Q}{2}) \quad \text{,where } n^2 = \varepsilon'_o \qquad (19)$$

The two signs refer to two circular waves.

## 2.3. Fresnel Reflection Coefficient

In the general case of reflection, the result of an inhomogeneous wave in an arbitrary direction must be combined with the general electromagnetic boundary conditions. For simplicity, we shall confine our attention to the case when the separating boundary, two media and the plane of incidence are parallel or perpendicular to the internal magnetic induction B. The geometric laws of reflection and refraction can be deduced without introducing the specific form of the boundary conditions, from the fact that these conditions are homogeneous and linear in the components of the electromagnetic field. It follows that if we use $E = E_o\, e^{(-i\omega t + i\omega \frac{\alpha^* x + \beta^* y + \gamma^* z}{v^*})}$ then $\frac{\alpha^* x + \beta^* y + \gamma^* z}{v^*}$ should be the same on the boundary for incident, reflected and refracted waves. In particular, if the boundary lies in the xy-plane while the xz-plane is the plane of incidence both for the plane of equal phase and the plane of equal amplitude, then $\alpha^*/v^*$ should be the same for all three waves, $\beta^*$ should be zero and $\alpha^{*2} + \gamma^{*2} = 1$. We shall confine our attention to the case of a homogeneous wave incident from an isotropic transparent medium (e.g. vacuum or air). In these conditions $\alpha^*$ and $v^*$ are real both in the incident and reflected waves and $v^*$ is the same for both waves. Since $\alpha^*/v^*$ is constant for both waves, the magnitudes of $\alpha^*$ (i.e. the sines of the real angle

of incidence and reflection) should also be equal. The corresponding values of $\alpha^*$ will be denote by $\alpha$. The angle of $\gamma^*$ should then have different signs for the two waves since otherwise the waves would be identical.

From Fresnel scattering theory, we have the following form for the reflected light

$$\begin{pmatrix} R_p \\ R_s \end{pmatrix} = \begin{pmatrix} r_{pp} r_{ps} \\ r_{sp} r_{ss} \end{pmatrix} \begin{pmatrix} A_p \\ A_s \end{pmatrix} \qquad (20)$$

where $A_p$ and $A_s$ are the incident light components parallel and perpendicular to the plane of incidence respectively, $R_p$ and $R_s$ are the components in the reflected light parallel and perpendicular to the incidence plane respectively. Only $r_{ps}$ and $r_{sp}$ are proportional to Q and giving us all the Kerr effects, while $r_{ss}$ and $r_{pp}$ can be used to describe the general optical properties of a metal surface.

As an example of Fresnel coefficients calculation, let us consider the polar Kerr effect. In this case the **M** is perpendicular to the sample surface. Suppose that a circularly polarized light is incident at an angle $\theta$ on a perpendicularly magnetized ferromagnetic film (xz plane is the incidence plane, xy plane is the plane of sample surface). Let us resolve the circular vibration into two: one elliptical and in the plane of the sample, and the other linear and perpendicular to the sample surface (parallel to **M**) and therefore not

contributing to the magneto-optical Kerr effect. The elliptical vibration is the projection of the circular vibration on to the plane of the sample surface and can be represented approximately by[2.6(P293)]

$$A_p = \pm i \frac{n\cos\theta + \cos\theta'}{n\cos\theta' + \cos\theta} A_s \qquad (21)$$

where $\theta'$ is the complex angle of refraction. At normal incidence $\theta = 0$ and the elliptical vibration described by (21) becomes circular. The amplitudes of the reflected light are then given by

$$R_{s\pm} = A_s \left( r_{ss} \pm i \frac{n\cos\theta + \cos\theta'}{n\cos\theta' + \cos\theta} r_{sp} \right) \qquad (22)$$

$$R_{p\pm} = A_p \left( r_{pp} \mp i \frac{n\cos\theta' + \cos\theta}{n\cos\theta + \cos\theta'} r_{ps} \right) \qquad (23)$$

In the absence of magnetization, $r_{sp} = r_{ps} = 0$. We have the Fresnel formulae for a general metal surface[2.6(P30)]

$$\left(\frac{R_s}{A_s}\right)_{Q=0} = r_{ss} = \frac{\cos\theta - n\cos\theta'}{n\cos\theta' + \cos\theta} \qquad (24)$$

$$\left(\frac{R_p}{A_p}\right)_{Q=0} = r_{pp} = \frac{n\cos\theta - \cos\theta'}{\cos\theta' + n\cos\theta} \qquad (25)$$

If the sample is magnetized and we want to know the equivalent formula, we must replace n by $n^*_{\pm}$ which we have from equation (19).

$$\left(\frac{R_s}{A_s}\right)_{\pm} = r_{ss} = \frac{\cos\theta - n^*_{\pm}\cos\theta'}{n^*_{\pm}\cos\theta' + \cos\theta} \qquad (26)$$

$$\left(\frac{R_p}{A_p}\right)_{\pm} = r_{pp} = \frac{n^*_{\pm}\cos\theta - \cos\theta'}{\cos\theta' + n^*_{\pm}\cos\theta} \qquad (27)$$

Substituting (19) into (26) and (27), and comparing with (22) and (23), we obtain, after simple transformations,

$$r_{sp} = r_{ps} = \frac{inQ_p\cos\theta\cos\theta'}{(\cos\theta + n\cos\theta')(n\cos\theta + \cos\theta')} \qquad (28)$$

where $Q_p = \gamma^* Q$. Since for majority metals, including ferromagnetic materials, $n^2 > 1$, it follows that

$$\gamma^* = \cos\theta' = \sqrt{1 - \alpha^{*2}} = \sqrt{1 - \frac{\alpha^2}{n^2}} \approx 1 \qquad (29)$$

So we have the following Fresnel coefficients for the polar Kerr effect

$$r^p_{pp} = \frac{n\cos\theta - 1}{n\cos\theta + 1}$$

$$r^p_{ss} = \frac{\cos\theta - n}{\cos\theta + n} \qquad (30)$$

$$r^p_{ps} = r^p_{sp} = \frac{inQ_p\cos\theta}{(\cos\theta + 1)(n\cos\theta + 1)},$$

where the superscript "p" represents polar Kerr effect.

In the similar way we can get the Fresnel coefficients for the Longitudinal and Transverse Kerr effects.

For longitudinal Kerr effect, we have

$$r^l_{pp} = \frac{n\cos\theta - 1}{n\cos\theta + 1}$$

$$r^l_{ss} = \frac{\cos\theta - n}{\cos\theta + n} \qquad (31)$$

$$r^l_{ps} = - r^l_{sp} = \frac{inQ_l\cos\theta\sin\theta}{(\cos\theta + n)(n\cos\theta + 1)}$$

where the superscript "l" represents the longitudinal Kerr effect.

For the Transverse Kerr effect, we have

$$r^t_{pp} = \frac{n\cos\theta - 1}{n\cos\theta + 1}\left(1 + \frac{iQ_t\sin(2\theta)}{n^2\cos^2\theta - 1}\right)$$

$$r^t_{ss} = \frac{\cos\theta - n}{\cos\theta + n} \qquad (32)$$

$$r^t_{ps} = r^t_{sp} = 0$$

where the superscript "t" represents the transverse Kerr effect.

We know that we always get combined Kerr effects in a oblique incidence situation. But we should notice that all three kinds of Kerr effects are functions of incident angle. When the incident angle $\theta = 0$, the longitudinal and the transverse Kerr effect disappear. Only the polar Kerr effect is not equal to zero when $\theta = 0$.

## 2.4. Experimental Signals

Our Kerr effect experimental apparatus is shown in Fig 3.1. The remaining analysis focuses on the relation between the intensity detected by a photodiode and the polarizer - analyzer angles. We denote the angle of the transmission axis of the polarizer as $\theta_p$ and the angle of the analyzer as $\theta_a$. For an observer looking toward the photon source, the angle are defined to be positive (negative) for a counterclockwise (clockwise) rotation from the plane of incidence; See Fig.2.2, where the S axis is perpendicular to the incident plane, and the P axis is in the plane of incidence.

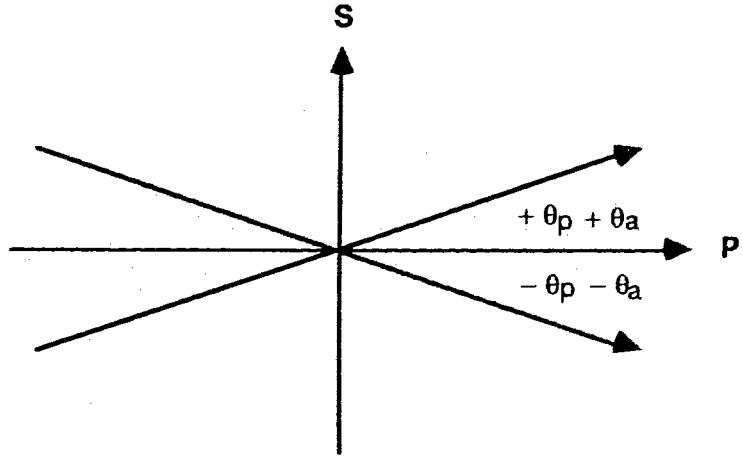


Fig.2.2

The electric field of the incident light after transmission through the polarizer has the vector form

$$\mathbf{E} = E_o\cos\theta_p\hat{\mathbf{P}} + E_o\sin\theta_p\hat{\mathbf{S}} \qquad (33)$$

where $\hat{\mathbf{P}}$ denote the unit vector parallel to the plane of incidence and $\hat{\mathbf{S}}$ denote the unit vector perpendicular to the plane of incidence.

From the Fresnel theory, for the combined magneto-optical Kerr effects, the reflected electric vector E' from the sample surface is in the form[1.5]

$$\mathbf{E'} = S^t(Q_t)\mathbf{E} + S^p(Q_p)\mathbf{E} + S^l(Q_l)\mathbf{E} \qquad (34)$$

where $S^t$, $S^p$ and $S^l$ are the scattering matrices for transverse, polar and longitudinal Kerr effect respectively. They are

$$S^t(Q_t) = \begin{pmatrix} r^t_{pp}(Q_t) & 0 \\ 0 & r^t_{s\,s} \end{pmatrix}, \quad S^p(Q_p) = \begin{pmatrix} r^p_{pp} & r^p_{ps}(Q_p) \\ r^p_{sp}(Q_p) & r^p_{s\,s} \end{pmatrix}$$

$$S^l(Q_l) = \begin{pmatrix} r^l_{pp} & r^l_{ps}(Q_l) \\ r^l_{sp}(Q_l) & r^l_{s\,s} \end{pmatrix} \quad ; \qquad (35)$$

where $Q_t$, $Q_p$ and $Q_l$ are proportional to $M_t$, $M_p$ and $M_l$ respectively. We also know that[2.5]

$$Q_j = \frac{4\pi}{i\varepsilon'_o}\left(\alpha + \frac{\sigma}{i\omega}\right) = Q_{jo}(M_j) + iQ'_j(M_j), \qquad j = t,\ p,\ l \qquad (36)$$

$$\mathbf{M}^2_t + \mathbf{M}^2_p + \mathbf{M}^2_l = \mathbf{M}^2_s \ , \qquad (37)$$

where $M_S$ is the total magnetization. Substituting (33) into (34), we have

$$E'_p = (r^t_{pp} + r^l_{pp} + r^p_{pp})E_p + (r^l_{ps} + r^p_{ls})E_s \qquad (38)$$

$$E'_s = (r^l_{sp} + r^p_{sp})E_p + (r^t_{ss} + r^l_{ss} + r^p_{ss})E_s \qquad (39)$$

The reflected light is sent to the analyzer where only the component parallel to the analyzer transmission axis will pass. This transmitted component is subsequently sensed by a photodiode. The transmitted light after the analyzer is[2.7]

$$E_t = E'_s \sin\theta_a + E'_p \cos\theta_a \qquad (40)$$

In our experimental system we take $E_s \approx 0$, because $\theta_p = 0$. So we have

$$E_t = [r^l_{sp}(Q_l) + r^p_{sp}(Q_p)]E_o \sin\theta_a + [r^t_{pp}(Q_t) + r^l_{pp} + r^p_{pp}]E_o \cos\theta_a \qquad (41)$$

The output current from a photodiode sensing this light is proportional to the modulus squared of equation (41). Thus the resulting expression for the detected signal, normalized to the incident intensity, is

$$\left(\frac{E_l}{E_o}\right)^2 = \left(Re\left(\frac{E_t}{E_o}\right)\right)^2 + \left(Im\left(\frac{E_t}{E_o}\right)\right)^2 \qquad (42)$$

where

$$Re\left(\frac{E_l}{E_o}\right) = \left(\frac{Q'_l \sin\theta\cos\theta}{(n\cos\theta + 1)(\cos\theta + n)} + \frac{nQ'_p}{(\cos\theta + n)(n\cos\theta + 1)}\right)\sin\theta_a +$$

$$(r^l_{pp} + r^p_{pp})\cos\theta_a + \frac{n\cos\theta - 1}{n\cos\theta + 1}\cos\theta_a + \frac{(\sin 2\theta)Q'_t}{n^2\cos^2\theta - 1}\frac{n\cos\theta - 1}{n\cos\theta + 1}\cos\theta_a \qquad (43)$$

$$Im\left(\frac{E_l}{E_o}\right) = \left(\frac{Q_{lo}\sin\theta\cos\theta}{(n\cos\theta + 1)(\cos\theta + n)} + \frac{nQ_{po}}{(\cos\theta + n)(n\cos\theta + 1)}\right)\sin\theta_a +$$

$$\frac{(\sin 2\theta)Q_{to}}{n^2\cos^2\theta - 1}\frac{n\cos\theta - 1}{n\cos\theta + 1}\cos\theta_a \qquad (44)$$

If we substitute (43) and (44) into (42) and ignore the $Q^2$ and the $\cos^2\theta_a$ terms, because $\theta_a \approx 90^o$, we will find that our experimental system is sensitive only to one term

$$\left((r^l_{pp} + r^p_{pp}) + \frac{n\cos\theta - 1}{n\cos\theta + 1}\right)\left(\frac{Q'_l \sin\theta\cos\theta + nQ'_p}{(n\cos\theta + 1)(\cos\theta + n)}\right)\sin 2\theta_a \qquad (45)$$

This means that in the usual case, when the incident angle $\theta \neq 0$, the signal we get from our experimental system is a combined polar and longitudinal Kerr effect.

## 2.5. Discussion

The evidence from the experiment result shows that the hysteresis loop will change its sign when we change the angle of the analyzer $\theta_a$ to $-\theta_a$. Fig. 2.3 shows the results. This agrees with the equation (45).

From equation (45), we also see that our signal is proportional to $Q'_l$ and $Q'_p$. So the signal detected by the photodiode is only sensitive to the magnetization component parallel to the plane of incidence ($M_l$), and the magnetization component perpendicular to the sample surface ($M_p$). We also want to point out here that when the incident angle $\theta = 0$, the longitudinal Kerr effect will be eliminated. The signal is only from the polar Kerr effect. This permits us to distinguish between the two kinds of Kerr effects easily.

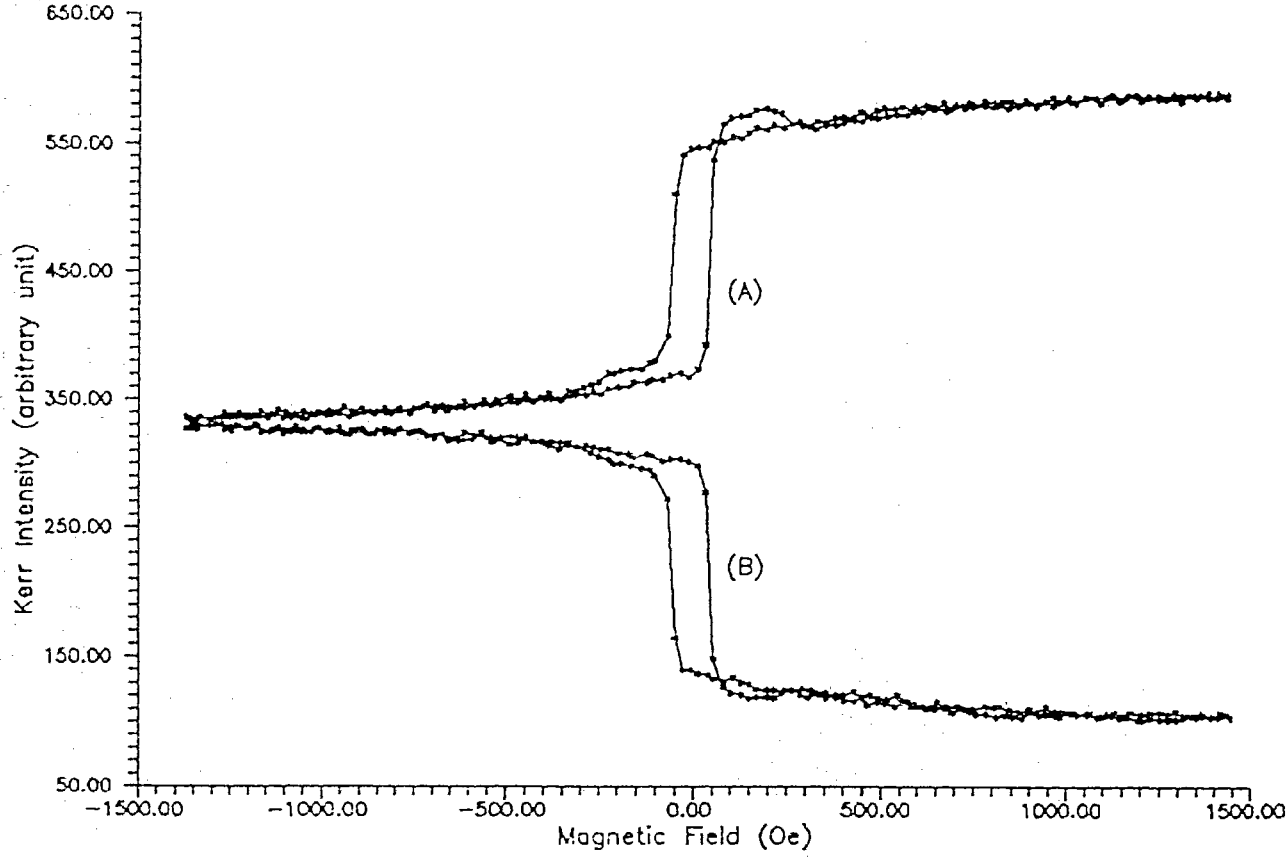


Fig.2.3 Hysteresis loop of 20MLAu/10MLNi/7MLFe/Ag(001) along its [11] hard axis. Loop (A) was measured by setting positive analyzer angle ($\Theta_a > 0$). Loop (B) was measured by setting negative analyzer angle ($\Theta_a < 0$).

## 2.6. References

[2.1] J. H. Judy, Proceedings, Conference on Advances in Magnetic Recording, N. Y. Acad. of Science 189, 239 (1972)

[2.2] M. J. Freiser, IEEE Trans. Mag-4, 152 (1968)

[2.3] R. P. Hunt, J. Appl. Phys. 38, 1652 (1967)

[2.4] C. C. Robinson, J. Opt. Soc. Am. 53, 681 (963)

[2.5] P.N. Argyres, "Theory of Faraday and Kerr Effects in Ferromagnetics", Physics Review, V97, 2, P334, (1955)

[2.6] A.V. Sokolov, "Optical Properties of Metals" (1961) p389

[2.7.] J.M. Florczak and E. Dan Dahlberg, "Detecting Two Magnetizaton Components by the Magneto-optical Kerr Effect"

[2.8.] Ronald F. Soohoo, "Magnetic Thin Films"

# Chapter 3

# Experimental Apparatus

## 3.1. Magneto-optical Kerr Effect System

Our experimental system has three parts. These are the Kerr effect system, the data acquisition system and the temperature controlling system. See Fig. 3.1. In order to understand the features and the operating procedures of the system, we explore each part in detail.

The Kerr effect system contains a 0.1mw He-Ne laser (0.01% Intensity drift/day), two low power glan laser prisms (Ealing part number MGLS/8/BB) with extinction ratio $<10^{-6}$ for $\lambda$ = 632.8nm, two nonmagnetic glass mirrors with 98% reflectivity for He-Ne laser light, a quarter-wave plate, a photodiode module (Ealing Scientific Ltd. 28-8209), a function generator, a ±20 ampere bipolar power supply, a gauss meter and an electromagnet.

One prism is used as the polarizer and the other as the analyzer. The photodiode response time was tested by using chopped laser light. For this square wave signal we measured the photodiode output on the oscilloscope. (See Fig. 3.2) The photodiode response time is

$$\Delta T \approx 0.1 \text{ ms} \qquad (3.1)$$

This response time is good enough for us. The typical magnetic field sweeping frequency in our experiments is about 0.06 Hz.

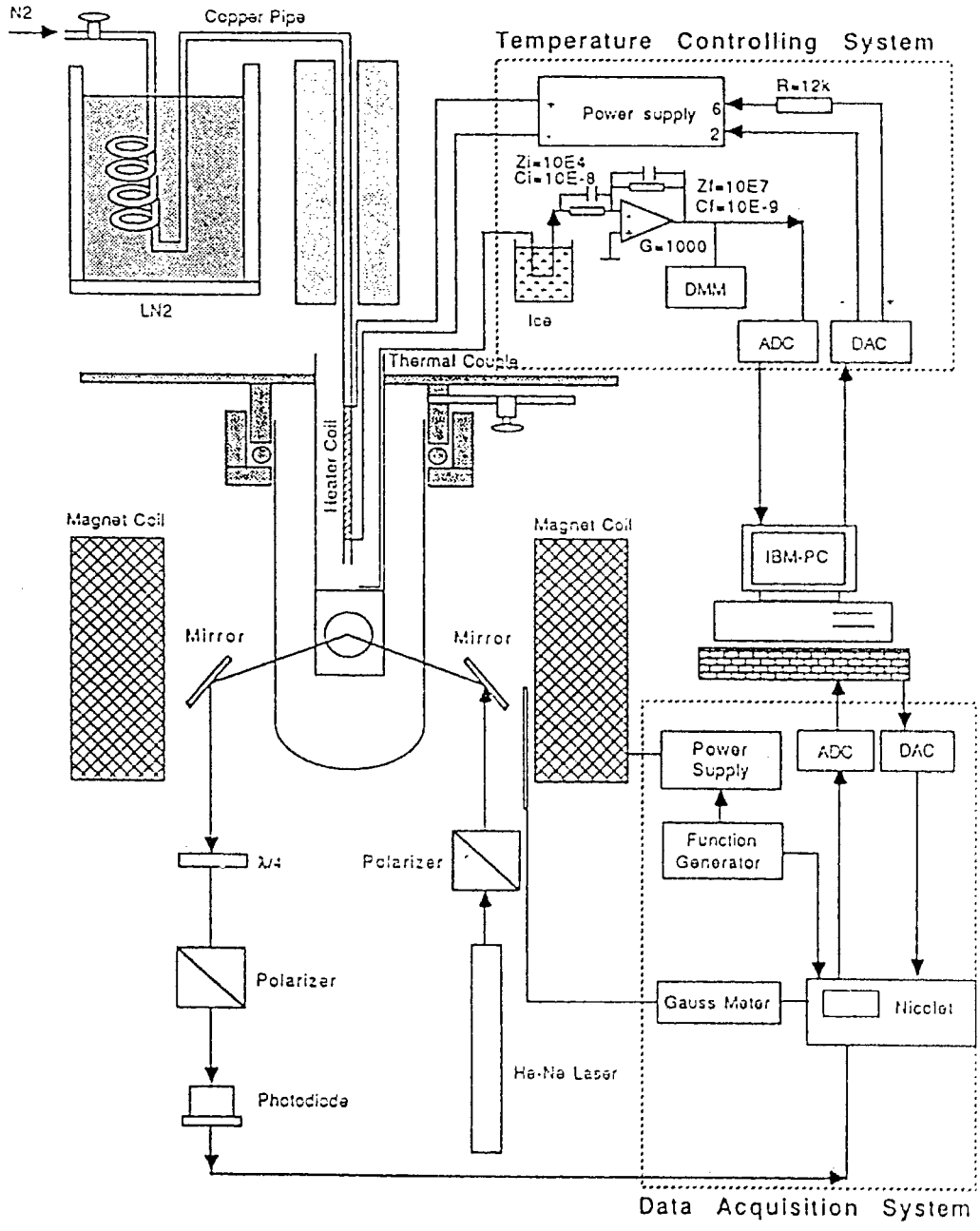


Kerr Effect System

Fig. 3.1 Note: The plane of the sample holder is perpendicular to the incident plane of the light.

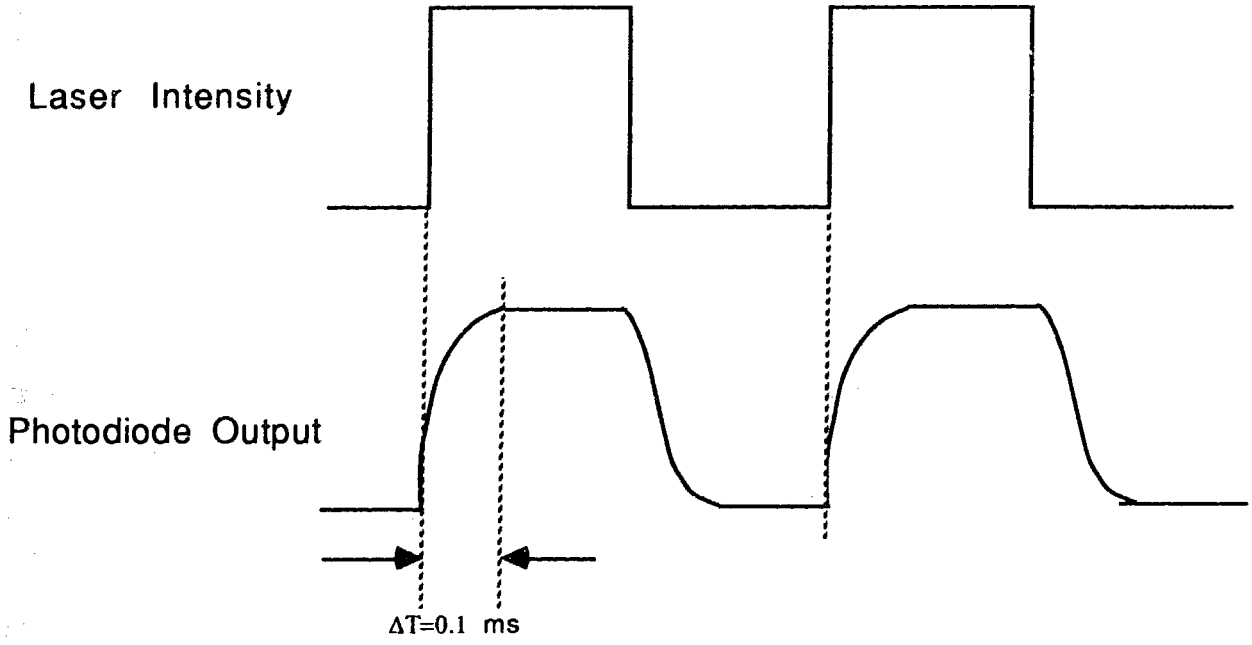


Fig.3.2

The data acquisition system includes an IBM-XT computer, a lab-master ADC/DAC interface and a Nicolet digital multichannel data logger. This part is controlled by the Kerr effect data processing program (KEDP.ZQM, See Appendix 1). The functions of this program are to transfer the Kerr effect data and the magnetic field data from the Nicolet digital data logger into the computer memory and to generate two data files on the floppy disk. This program also can generate a graphic file in the standard format of the TELEGRAPH program.

In order to get the hysteresis loop of a sample, we need to measure the Kerr effect signal vs external magnetic field. During

each measurement the magnetic field is provided with a ±20A power supply. The power supply is driven by a triangle signal from the function generator. The sweeping frequency of the magnetic field can be easily controlled.

The Nicolet data logger will start to collect Kerr effect data from the photodiode after receiving a trigger signal from the function generator in each period of the sweep. The Dwell time constant on the Nicolet should be adjusted to match the magnetic field sweeping period. See Fig.3.3. In the real case we always have a short dead time, because it is very hard to make the Dwell timeX1024 exactly equal to the magnetic field sweeping period. This means we may lose some data during each period, but we still get a fully closed hysteresis loop. The Nicolet data logger has 1024 channels, each channel will measure the average Kerr signal during the dwell time.

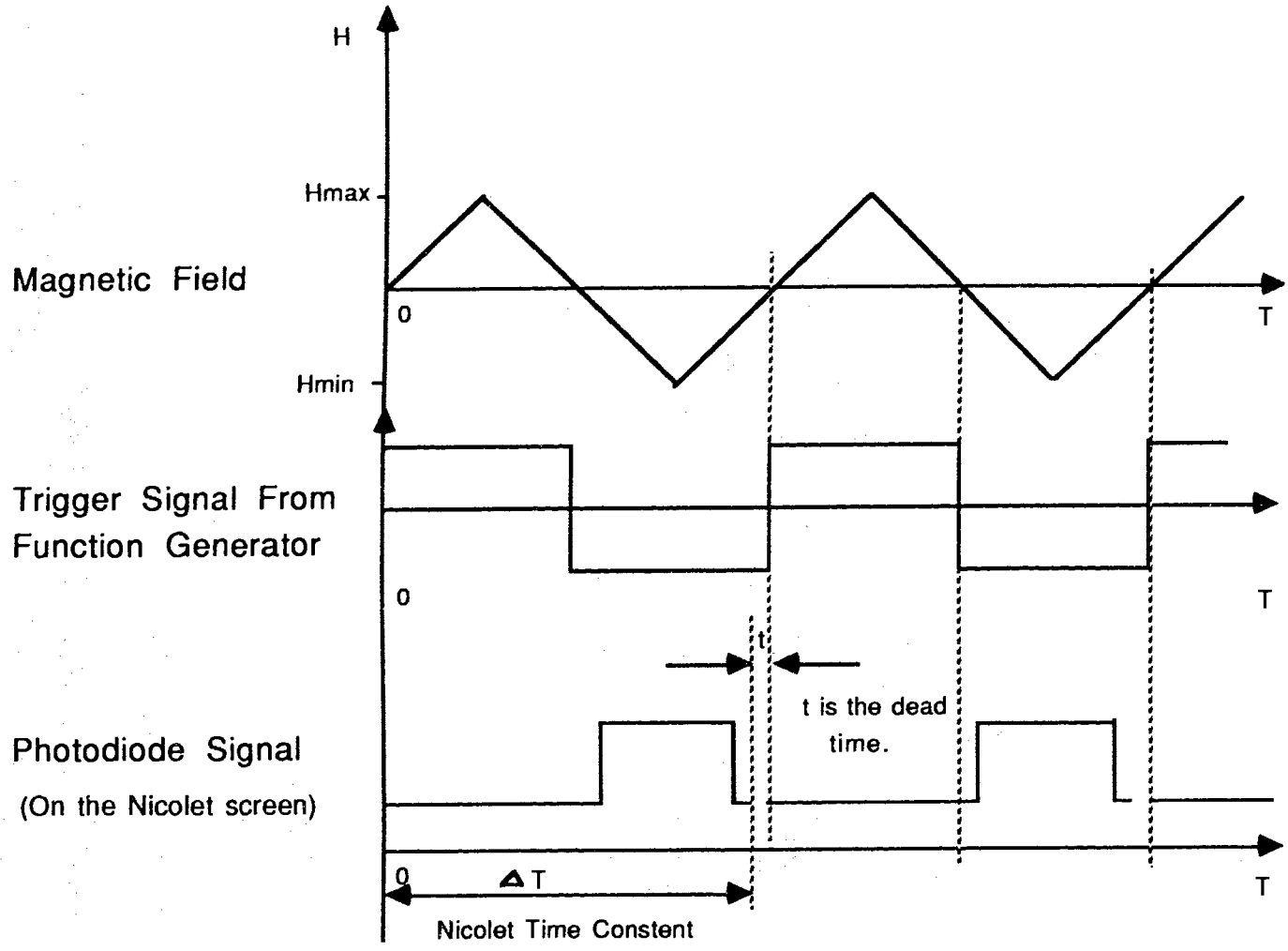


Fig.3.3

The Gauss meter we use has an output signal proportional to the magnetic field. The output signal range is +/-1(V) corresponding to positive and negative field at full range. Without changing the frequency of the function generator, we can collect the magnetic field data from the Gauss meter in the same way we collect the Kerr effect data. Because the Kerr effect signal and the magnetic field

are both measured one after the other in the same time scale, we can neglect the drift of the function generator. We can use them as X and Y data to get the final hysteresis loop.

Before measuring the magnetic field, we need to reset the Gauss meter. The probe is put into a magnetic field shield and the Gauss meter is set to zero, the Nicolet is set in the auto trigger mode, the MEASURE button is pushed and the offset is adjusted until the scanning spot is at the central line of the screen. This will be the zero field reading. The full scale output from the Gauss meter has been pre-measured. Both reading numbers are used in the Kerr Effect Data Processing program (KEDP.ZQM) for the magnetic field calibration. For different samples the required magnetic field strength may be different. Using the following equation we can get the true magnetic field value for different full range scale setting.

$$\text{Magnetic field value} = \frac{(\text{Measured value - zero reading})}{\text{Full scale reading}} * \text{Range},$$

where the Range is the full scale number on the Gauss meter. The whole procedure of the data measurement is given in Appendix 2.

The temperature controlling system is used during the low temperature measurement. This part includes a vacuum sample holder, a thermocouple, a pre-amplifier, a digital multimeter, a computer interface, a heater coil and its power supply.

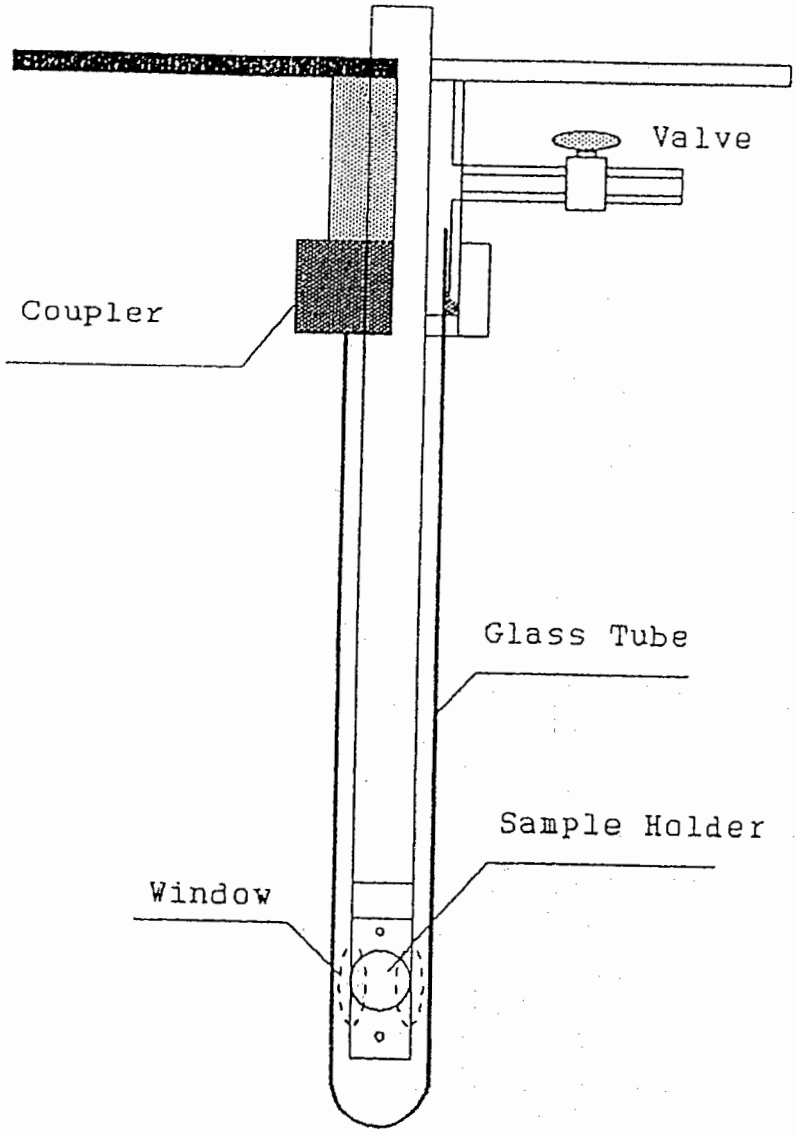


Fig.3.4

Fig.3.4 shows the specially designed vacuum sample holder. The Kerr signal is measured through two crystal windows on the glass tube.

The idea is to use liquid nitrogen to cool down the flowing nitrogen gas which is at the constant pressure of the central supply. This cold nitrogen gas blew directly to the copper sample holder (see Fig.3.1). The sample holder has very good thermal contact with the sample, so we assume that the sample has the same temperature as the sample holder after a very short time. A thermocouple is placed on the sample holder inner surface. The computer read the signal, compared it with a calibration table and displayed the calculated temperature on its screen. The Temperature Control Program TCTRL.ZQM (see Appendix 3) monitors the difference between the measured and the desired temperature. The computer uses this number as a parameter to control the output current of the heater power supply to keep the temperature at the desired value. The temperature can be controlled between room temperature and liquid nitrogen temperature. The fluctuations will be within two degrees Celsius. Fig.3.5 shows the logic structure of the temperature controlling program.

# Logic of Temperature Control Program

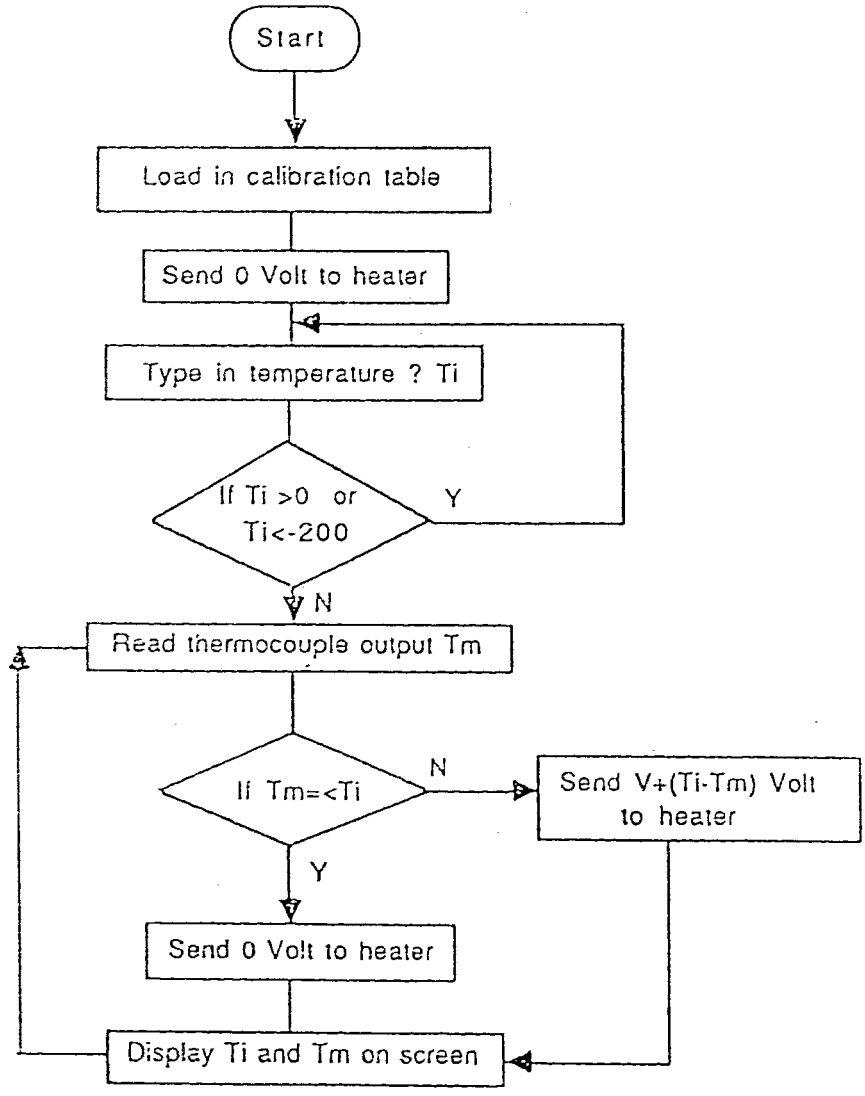


Fig. 3.5

## 3.2. Experiment Setup Procedures

The optical path should be setup carefully. In our experiment we set the polarizer axis parallel to the incident plane ($\theta_p = 0$ in Fig. 2.3), we denote it as P-polarized light. The incidence angle is about 45 degree to the sample surface normal. Suppose the reflected light is linearly polarized, and the angle between the analyzer axis and the reflected $E_r$ vector is $\theta_a$. The intensity after the analyzer will be

$$E^2_t = E^2_r \cos^2\theta_a \qquad (3.2)$$

so we have for the variation signal with Kerr effect

$$\Delta E^2_t = \Delta E^2_r \cos^2\theta_a - E^2_r (\sin 2\theta_a)\Delta\theta_a \qquad (3.3)$$

$\Delta E^2_r$ is the laser intensity drift noise and $\Delta\theta_a$ is the Kerr rotation. Then we have the signal to noise ratio

$$SNR = \frac{E^2_r \sin 2\theta_a \Delta\theta_a}{\Delta E^2_r \cos^2\theta_a} \qquad (3.4)$$

It is clear that we will have the SNR maximum when $\theta_a = \pi/2$. So the analyzer should be set with its axis perpendicular to the $E_r$ vector. In order to get a detectable signal, we always set the analyzer angle $\theta_a$ at about ten minutes away from the $\pi/2$ position.

The experiment results shows that the signal to noise ratio is good enough in this set up.

### 3.3. Sample Preparation

The samples we used in our experiments are prepared by using MBE (molecular beam epitaxy) techniques. A more detailed account of the Model 400 MBE equipment can be found in the thesis of Chian Liu[3.1]. The layout of the system is shown in Fig.3.6.

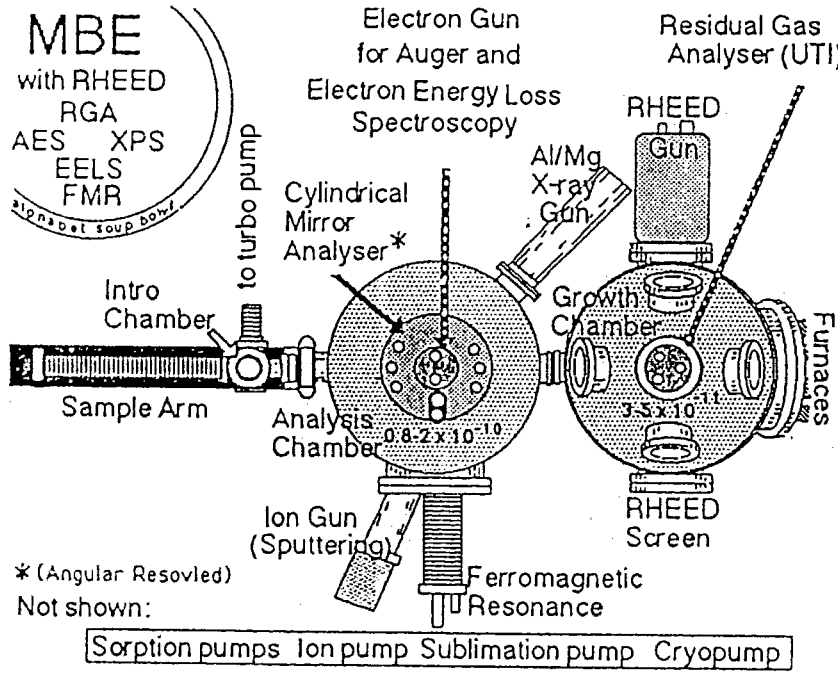


Fig.3.6

The MBE machine is formed by two interconnected vacuum chambers, one for XPS (X-ray Photoelectron Spectroscopy) and AES (Auger Electron Spectroscopy) analysis and one for growth. The vacuum is maintained by an ion pump connected to the analysis chamber and a cryogenic pump connected to the growth chamber. The background pressure was ≈ (4-8)x$10^{-11}$ Torr when no evaporation furnaces were turned on and ≈ 5x$10^{-10}$ Torr during evaporation.

A good epitaxial growth is anticipated when the overlayer and substrate lattices are well matched. Various types of lattice matching are possible. Samples we used in our Magneto-optical Kerr effect experiments are the Ni/Fe bilayers epitaxially growth on Ag(001). The Fe overlayers can be grown on Ag(001) surface because their lattices are well matched. Fig.3.7 shows the lattice relationship between bcc Fe and fcc Ag substrate.

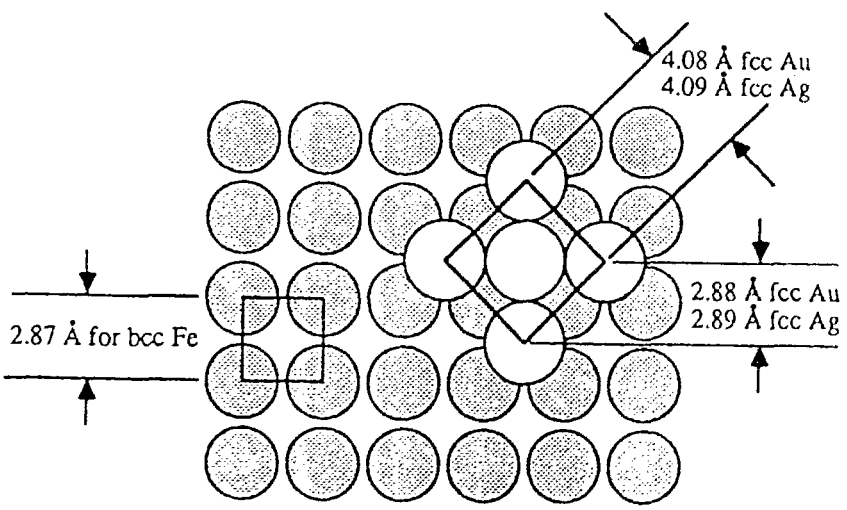


Fig.3.7

We also know that there is an appreciable vertical mismatch due to the large tetragonal distortion between the bcc and fcc lattices. In that case substrate steps become sources of defects and these defects will affect the growth and magnetic properties of Fe on Ag(001)[3.2].

The growth of Ni on ultrathin Fe(001) on bulk Ag(001) was similar to the growth of Ni on bulk Fe(001)[3.2]. In the next chapter we will briefly review previous studies of Ni/Fe bilayers on Ag(001).

Because the Magneto-optical Kerr Effect experiments are carried on outside the MBE vacuum chamber, all the samples we used were covered by Au overlayers to prevent from oxidation. Studies have shown that the Au coverlayer will slightly decrease the anisotropy of the Ni/Fe bilayer [3.3].

## 3.4. REFERENCES

[3.1] C. Liu, "Ultrathin Metallic Films of Mn, AgMn and VMn Grown By Molecular Beam Epitaxy", Ph.D. thesis, Simon Fraser University, (1986).

[3.2] Stephen T. Purcell, "Structural and Magnetic Properties of Ultrathin Epitaxial Nickel Films Grown on Iron (001) Surfaces", Ph.D. thesis, Simon Fraser University, (1989)

[3.3] B. Heinrich, J. F. Cochran, A. S. Arrott, S. T. Purcell, K. B. Urquhart, "Development of Magnetic Anisotropies in Ultrathin Epitaxial Films of Fe(001) and Ni(001).

# Chapter 4

# Experimental Results and Discussions

## 4.1 Introduction

The magnetic and structural properties of Ni/Fe bilayers on Ag(001) have been studied by using in-situ reflection high energy electron diffraction (RHEED), Brillouin Light Scattering (BLS) and ferromagnetic resonance (FMR)[3.2]. Previous studies showed that the ultrathin "bcc Ni"/bcc Fe bilayers grown on Ag(001) single crystal substrates form new materials with unique magnetic properties of their own. We review those results here briefly.

The studies showed that for 3-5 atomic layers the Ni overlayers have close to the same structure as bcc Fe. These bcc Ni overlayers have no effect on the magnetic properties of the ultrathin bcc Fe layers. But as the Ni film thickness is increased above a critical thickness (3-6 monolayers, depending on the details of sample preparation) reconstruction of the Ni layers occurs. While Ni has the bcc structure on Fe, the lattice parameter forced upon Ni probably differs from that of relative minimum energy for homogeneous isotropic Ni. The accumulating strain is relieved by a lattice reconstruction probably as an array of misfit dislocations. It is possible that this lattice reconstruction is triggered by atomic steps on the Ag substrate surface. It was also argued that the network of misfit dislocations might cause an increased diffusion of

Ag substrate atoms to the sample surface. This effect might not be limited to the Ni overlayers but might propagate throughout the whole Ni/Fe bilayer structure.

Magnetic properties of the Ni/Fe bilayers were investigated using FMR and BLS. The lattice reconstructed "bcc Ni" overlayers created a large in-plane 4-fold anisotropy with the easy axis along the Fe(001) crystallographic direction. This is in sharp contrast with single Fe layers for which the 4-fold in-plane anisotropy decreases with the Fe layer thickness and becomes negligible in 3-4 ML (monolayers) thick films.

The new phase of the Ni/Fe bilayer on Ag(001) has become very interesting in surface physics. Many research works have been done by using different methods. For example, FMR is a very useful technique to study Ni/Fe bilayers, but this technique usually uses external magnetic field strengths sufficient to saturate the magnetization. In order to understand all the magnetic properties of the Ni/Fe bilayers, careful investigations were needed in the low field region. This is the reason we chose the technique of surface magneto-optical Kerr effect (SMOKE). In the following sections we will show some interesting results obtained with the SMOKE method.

## 4.2 Sample Description

In the study of the magnetic properties of Ni/Fe bilayers at room temperature and low temperature, the following samples have

(a) Hysteresis loops;

Sample NiFe(10/6.6):

One year old.

30MLAu(001)/10MLNi(001)/6.6MLFe(001)/Ag(001) substrate

Sample NiFe(10/7):

Newly grown sample measured less than three hours after growth.

20MLAu(001)/10MLNi(001)/7MLFe(001)/Ag(001) substrate

(b) Coercivity as a function of temperature

Sample Fe(9):

20MLAu(001)/9MLFe(001)/Ag(001)substrate

Sample NiFe(3/6):

20MLAu(001)/3MLNi(001)/6MLFe(001)/Ag(001)substrate

Sample NiFe(15/6):

20MLAu(001)/15MLNi(001)/6MLFe(001)/Ag(001)substrate

All these samples were grown on the same Ag substrate. A detailed inspection of Laue patterns revealed that its surface was not cut exactly parallel to the (100) surface. but had an average misorientation of 1.8 degree. The surface could be characterized as being close to the (3,1,33) atomic plane.

## 4.3 Hysteresis Loops of Ni/Fe Bilayers

In order to investigate the magnetic properties of Ni/Fe bilayers, the SMOKE technique was used successfully to measure hysteresis loops at low temperatures as well as at room temperature.

The most striking property of the Ni/Fe bilayers is the enhanced in-plane four-fold magnetic anisotropy that develops because of the reconstruction that takes place in the Ni overlayer when its thickness exceeds 5-7ML. If 7ML of Fe is not covered by the Ni, its in-plane anisotropy is reduced with respect to the bulk value of Fe. The FMR experiment shows that for the NiFe(10/6.6) sample the anisotropy at 300K exceeds that of bulk Fe, and at 77K it is four times that of bulk Fe.

Some results of hysteresis loops from the combined (longitudinal and polar) Kerr effects of NiFe(10/7) sample at room temperature are shown in Fig.4.1. The series of measurements starts with the sample's [10] easy axis parallel to the external field. When we rotate the sample, so that its easy axis is away from the external field direction, steps appear in the hysteresis loop, occurring at higher magnetization the further the sample is rotated. We get a very unusual hysteresis loop when the hard axis is parallel to the field direction. We see that these two jumps are in the same direction on both side, violating usual symmetry rules. At an other hard axis, 90 degree away, the two jumps are again on both sides of

the loop, but now the sign of the jumps is reversed.

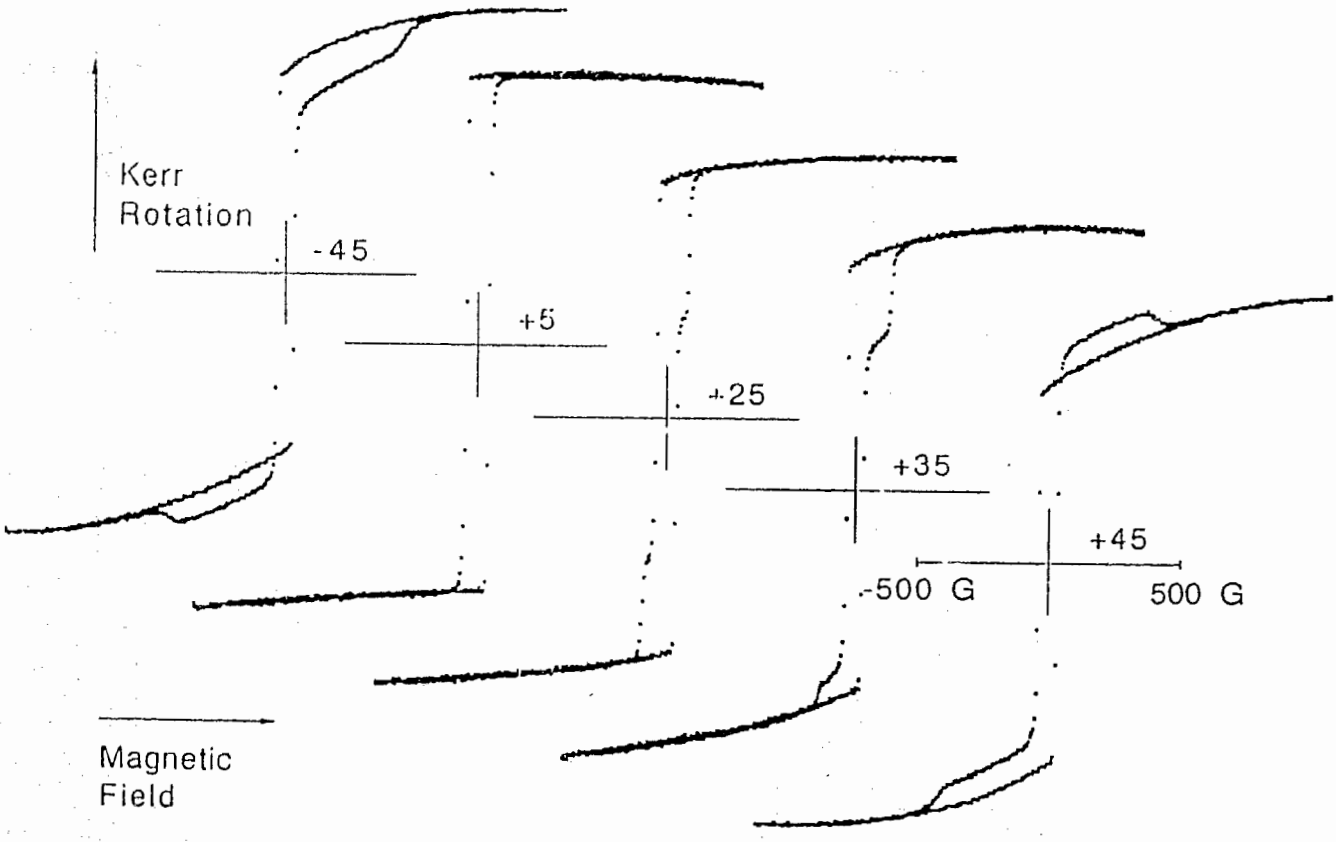


Fig.4.1 Hysteresis loops of 30MLAu/10MLNi/7MLFe/Ag(001) sample at room temperature. Angle measured between the [10] easy axis and the external field direction. Field sweeping frequency is 0.8Hz. The angle of Incidence is 45 degree.

We have carried out a number of variations of the experiments to convince ourselves that this lack of symmetry along the hard axis is not an artifact of the measurement, but really says that the sample has an unknown unidirectional anisotropy. The application of a 17KG fields parallel to the sample surface in several direction between measurement had no effect on those two jumps.

The coercivity is 37 Oe for the hard axis and 40 Oe for the easy axis.[4.1] The coercivity is found to be almost independent of the direction in the plane of the film.

The magnetic moment, measured at the departure field, along the hard axis was 1.38 ($\approx \sqrt{2}$ ) smaller than the corresponding magnetic moment along the easy axis. This indicates that the sample was fully saturated when it was magnetized along the easy axis and probably formed 90 degree stripe domains when the applied field was directed along the hard axis.[4.2]

We obtained the same results for the sample NiFe(10/6.6) at room temperature. Fig 4.2 shows that the hysteresis loop for the [10] easy axis is rectangular with a coercivity of 39 Oe. Fig 4.3 shows the hysteresis loop along [11] hard axis. For the hard direction the coercivity is 37 Oe.

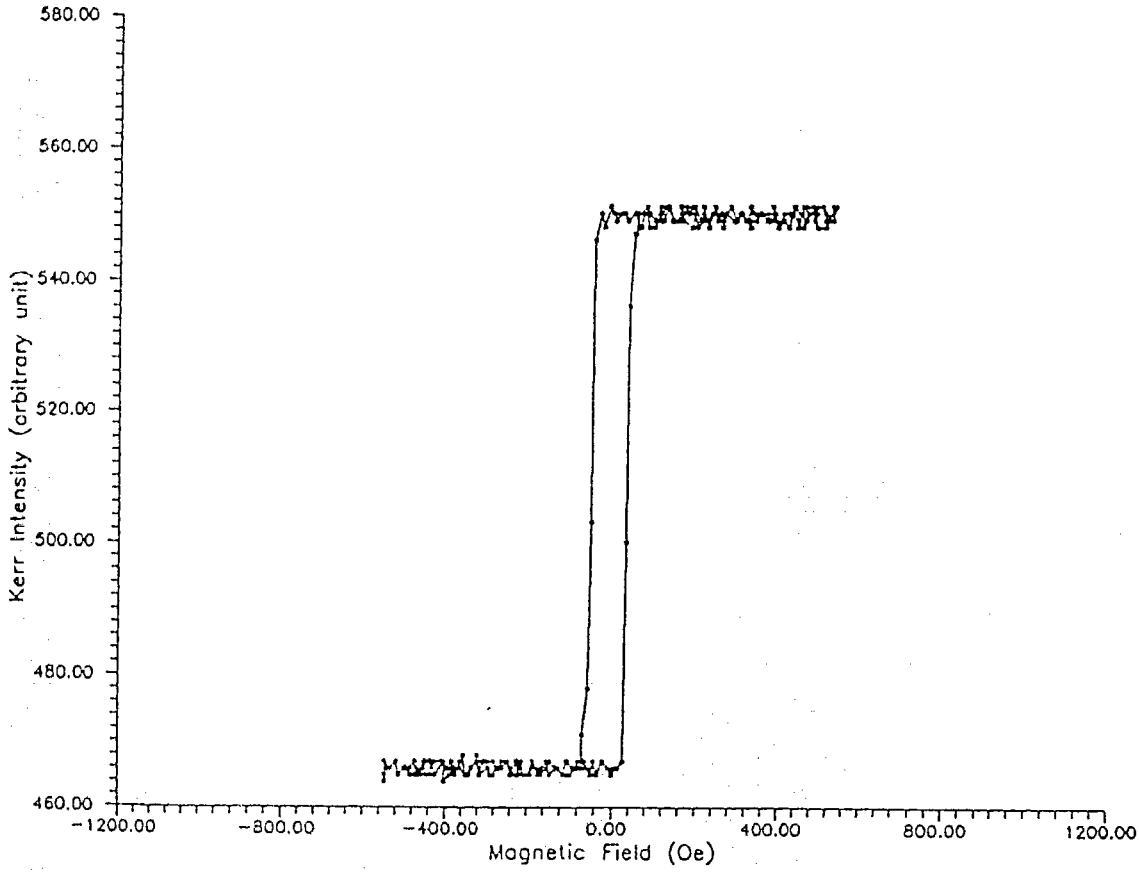


Fig.4.2 Hysteresis loop of 30MLAu/10MLNi/6.6MLFe/Ag(001) along its easy axis at room temperature. The angle of incidence is 45 degree. Field is swept at 0.8 Hz.

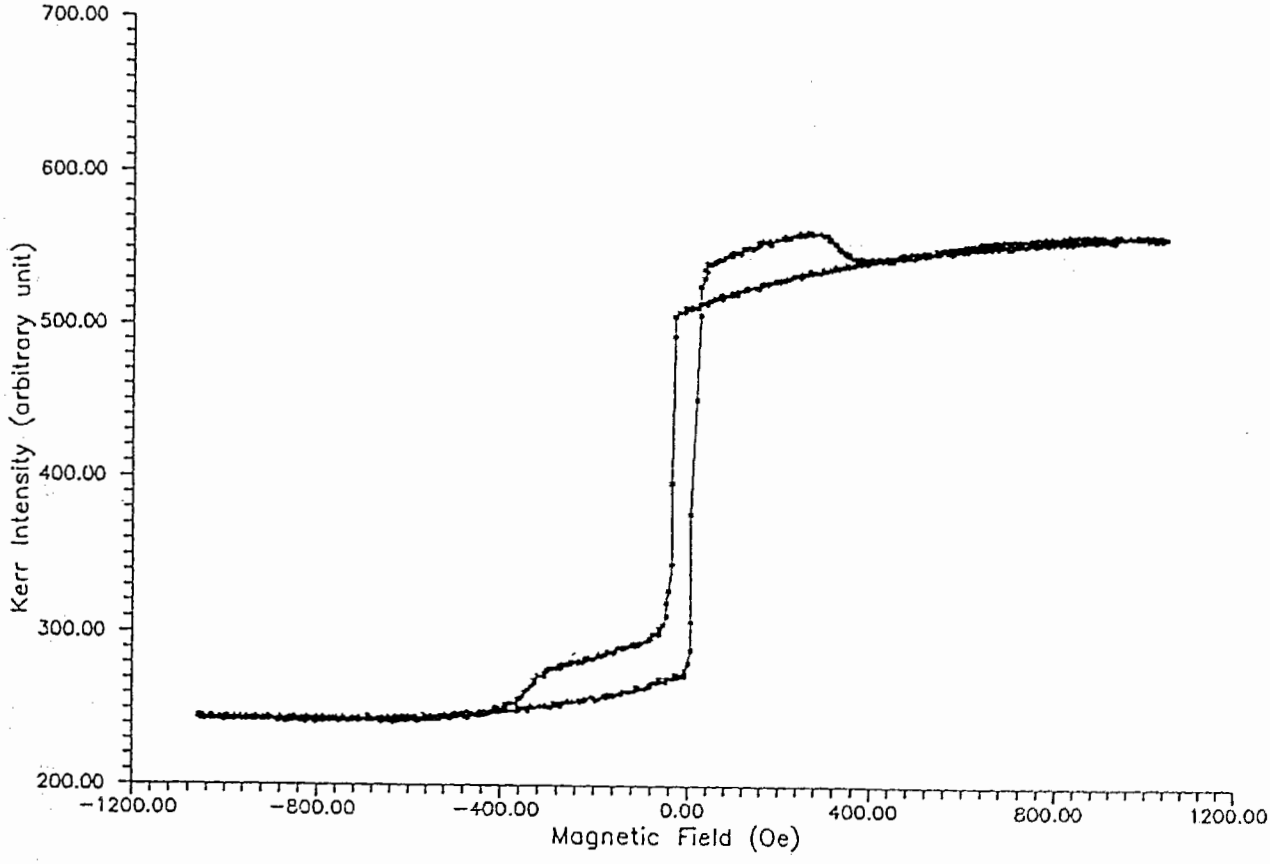


Fig.4.3 Hysteresis loop of 30MLAu/10MLNi/6.6MLFe/Ag(001) along its hard axis at room temperature. The angle of incidence is 45 degree. Field is swept at 0.8 Hz.

After eliminating many other possibilities on the source of the two asymmetric jumps, we checked to see if could be the result of a polar Kerr effect. Using sample NiFe(10/6.6), we first set the sample with one of its hard axes along the external magnetic field and measured the combined Kerr effect as we did before. Without changing the sample's orientation, we rearranged the system to make the laser beam perpendicular to the sample surface. The system setup for the polar Kerr effect measurement is shown in Fig.4.4. The polar Kerr effect and the combined Kerr effect results are shown together in Fig.4.5. It is very clear that the two small jumps are really coming from the polar Kerr effect. We can see that they are caused by a magnetization component perpendicular to the sample surface.

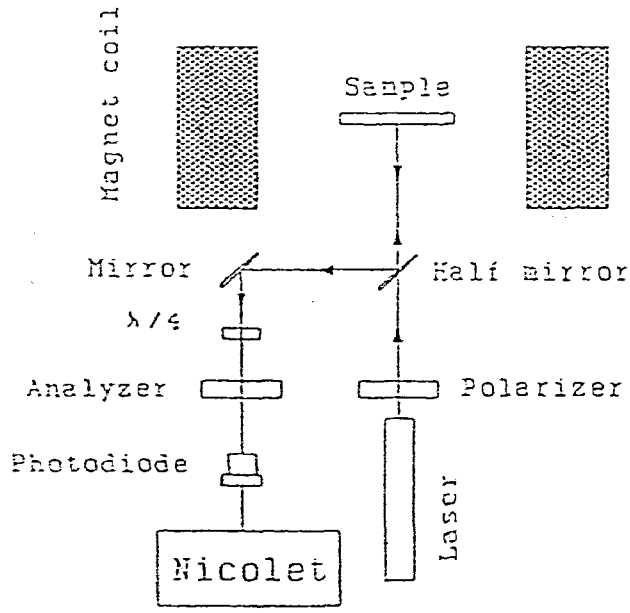


Fig.4.4 Experimental system for polar Kerr effect measurement of the magnetic field component perpendicular to the sample surface.

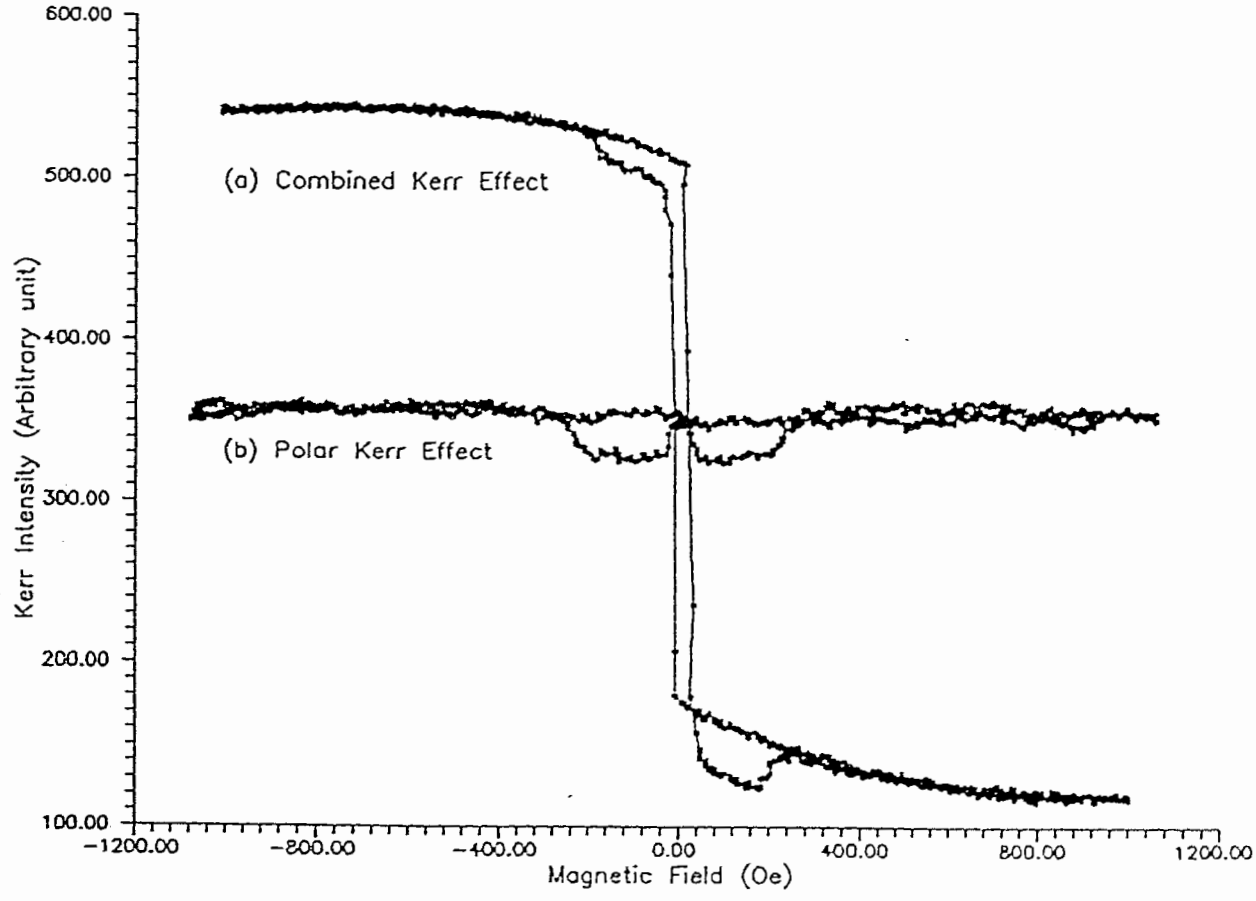


Fig. 4.5 Hysteresis loop of 30MLAu/10MLNi/6.6MLFe/Ag(001) along its hard axis at room temperature. Field swept at 0.8Hz. (a) Combined Kerr effect result. The angle of incidence is about 45 degree. (b) Polar Kerr effect result.

## 4.4 Coercivity as a Function of Temperature

As we pointed out in the last chapter, the coercive force for the hard and easy axis were almost the same at room temperature for the sample NiFe(10/6.6) as well as for the sample NiFe(10/7). If this unusual result were to be explained by competing mechanisms, then it is likely that changing the temperature would make some difference. We designed a temperature controlling system and a vacuum sample holder for determining the effect of temperature on the hysteresis loops. This experimental apparatus was shown in chapter 3. All the experiments started from room temperature (21 C) and cooled down to liquid nitrogen temperature. The hysteresis loops for fixed sample orientation are measured at a series of temperatures.

First we have measured the pure iron sample 20MLAu /9MLFe/Ag(001). Its coercive force along its easy axis is about 15.5 Oe at room temperature. When the temperature decreases towards to liquid nitrogen temperature, the coercive force increases almost linearly to 25.5 Oe. Fig.4.6 shows the result.

In order to see what kind of effect will be caused by Ni overlayers, we also measured the sample NiFe(3/6) in its easy axis orientation. The coercive force is 4 Oe at room temperature and increased by a factor of four to 16.5 Oe at liquid nitrogen temperature. Fig.4.6 shows that the lines for the two samples have about the same slope.

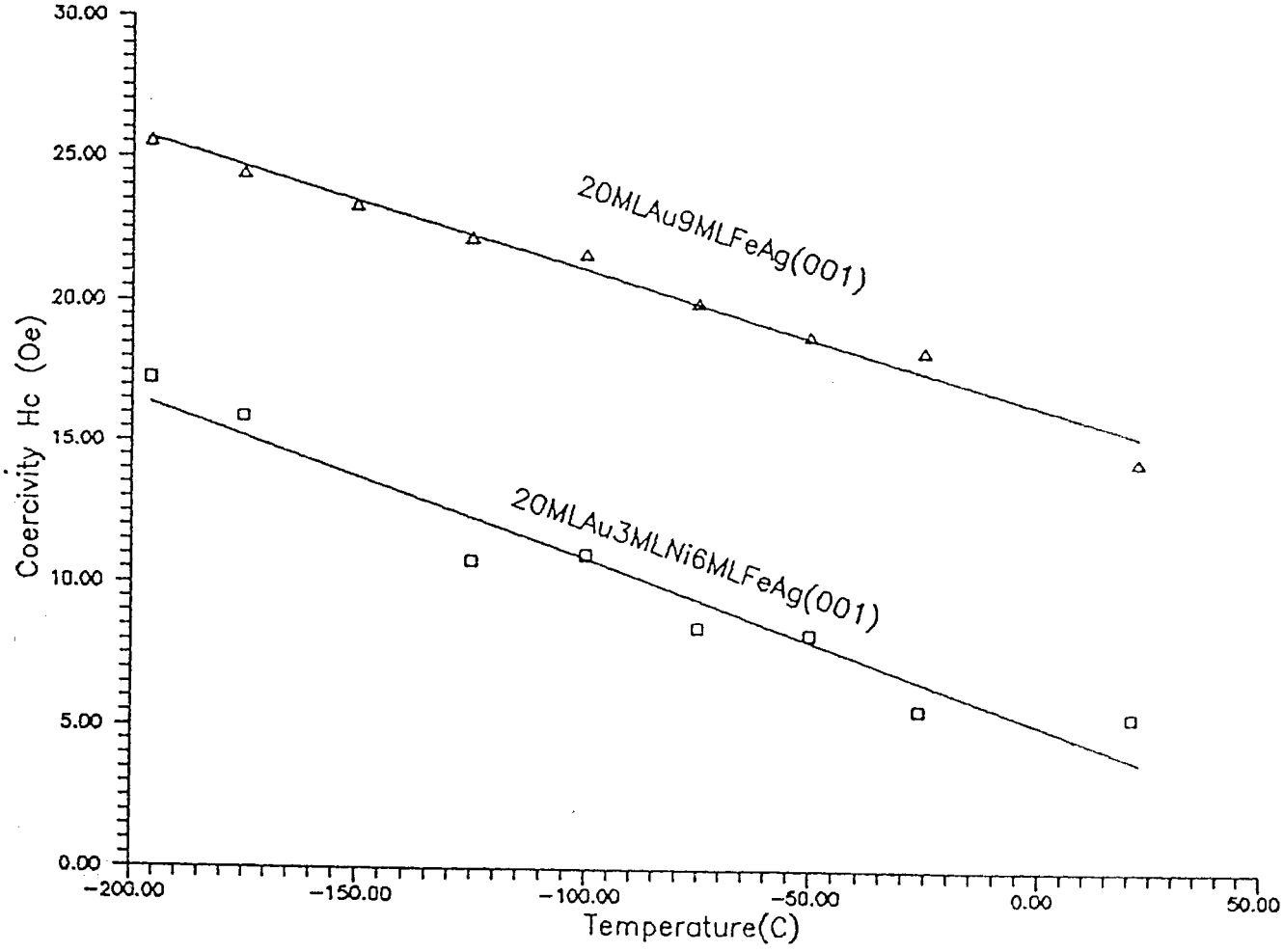


Fig.4.6 Coercive force as a function of temperature. Sample: 20MLAu/9MLFe/Ag(001) and 20MLAu/3MLNi/6MLFe/Ag(001). Orientation: Easy axis.

We also noticed that at -200 C the ratio of the two coercive forces is just about same as the ratio of numbers of monolayer Fe in each sample. This is additional evidence that un-reconstructed bcc Ni coverlayers have little effect on the magnetic properties of ultrathin Fe samples. This agrees with the results obtained by Heinrich et al. [4.2-4.3] from FMR.

There is much different behavior for the sample of NiFe(15/6). Fig.4.7 shown the results measured along the sample's hard and easy axes. The coercive forces on hard and easy axes are no longer the same at lower temperatures. Comparing the result of easy axis in Fig.4.7 with that of sample NiFe(3/6) in Fig.4.6, we see that the coercive force of the NiFe(15/6) bilayers increased by almost a factor of 30 due to the reconstructed Ni overlayers.

## 4.5 Discussion

We are particularly interested in strange effects that take place during the rotation process in the approach to saturation after the reversals in the magnetization for the field in the hard axis direction. From Fig.4.5, the pure Polar Kerr effect shows that signal to be symmetric for positive and negative fields. Starting from saturation in a hard (110) direction, the magnetization rotates in the plane toward the easy axis as the field is decreased. Before the instability point for uniform rotation is reached, there is a reversal by means of domain nucleation and growth. This structure has a magnetization component out of the plane which persists to a

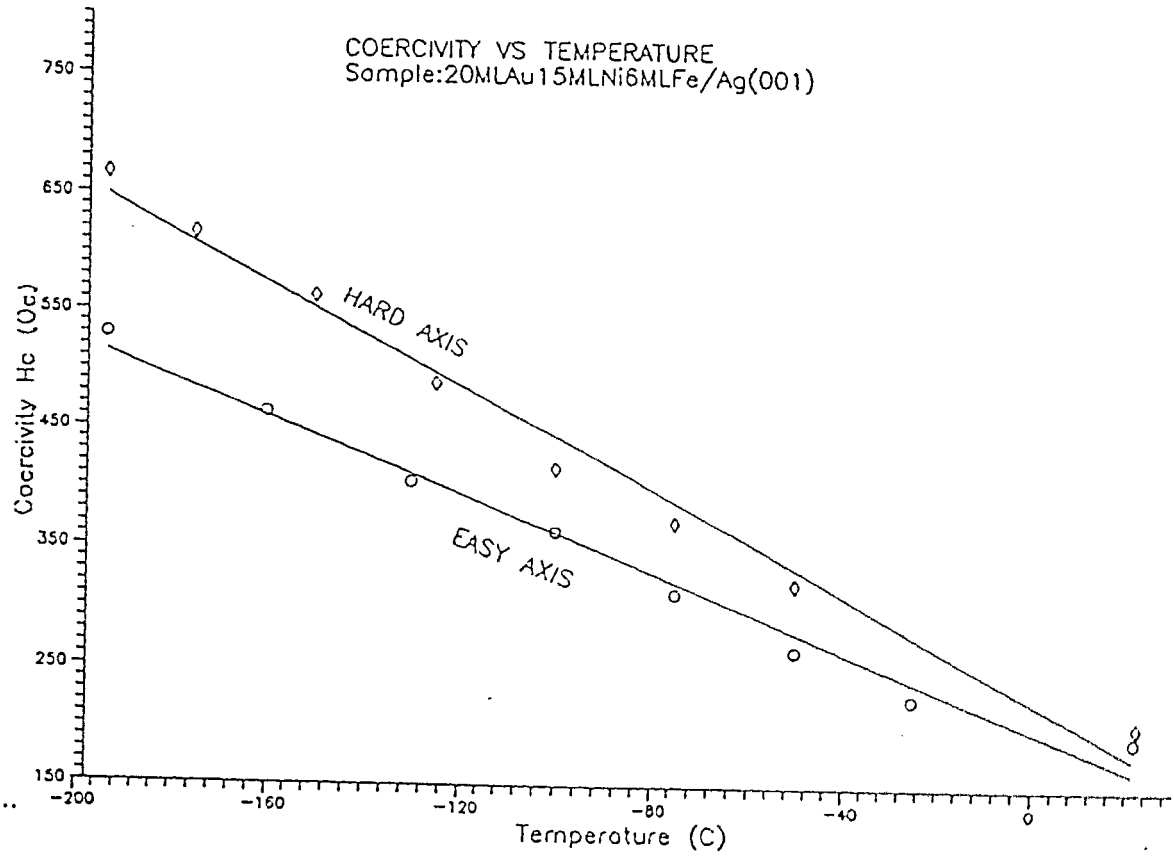


Fig.4.7 Coercive force as a function of temperature. Sample: 20MLAu/15MLNi/6MLFe/Ag(001).

critical field at which it reverts to the plane of the sample as saturation is approached in the reversed field. The same process is observed for fields changing from the reversed to the original sense. This unidirectional anisotropy is attributed to the freezing of some spin configurations during the epitaxial growth of Ni on the transformed structure.

Another problem is the independence of the coercivity upon direction of the field at room temperature. We notice that the sharpness of the transition and the fact that it is in a small field compared with the single-particle switching field for rotation. We might say that the reversal takes place by growth of domains, the walls of which become free to move in slightly negative fields. If the nucleated domain structure is, as found by Sato et al[4.4], predominantly a checkerboard pattern of 90 degree walls, then the fourfold symmetry of the pattern suggests that the field required to break the pinning of the walls may well be the same in all directions.

## 4.6 Conclusions

An unusual unidirectional anisotropy was found on the Ni/Fe bilayer sample in our surface magneto-optical Kerr effect experiment which is not found in FMR data. This unidirectional anisotropy might be caused by freezing some spin configurations during the epitaxial growth of Ni overlayers. The polar Kerr effect signal shows that this unidirectional anisotropy will make the

magnetization component always out of one side the sample plane during the approach to saturation. The microscopic mechanism of this saturation is not known. All the polar Kerr effect experiments were carried out at room temperature. It will be very interesting to investigate the polar Kerr signal at lower temperature.

Our results also show that the pure bcc Ni overlayers have little effect on the magnetic properties of ultrathin Fe samples. But the reconstructed Ni overlayers increased the coercivity 30 times. This can be explained by the strong fourfold in-plane anisotropy introduced by the reconstructed Ni overlayers. This agrees with the result from FMR.

## 4.7 Reference

[4.1] Q.M. Zhong, A.S. Arrott, B. Heinrich, and Z. Celinski, "Surface Magneto-optical Kerr Effect for Ultrathin Ni-Fe Bilayers", J. Appl. Phys. 67(9),1 May 1990.

[4.2] B. Heinrich, A. S. Arrott, J. F. Cochran, K. B. Urquhart, K. Myrtle, Z. Celinski, and Q. M. Zhong, "In-situ Techniques for Studying Epitaxially Grown Layers and Determining Their Magnetic Properties", Mat. Res. Soc. Symp. Proc. Vol. 151. 1989.

[4.3] B. Heinrich, S. T. Purcell, J. R. Dutcher, K. B. Urquhart, J. F. Cochran, and A. S. Arrott, "Structural and Magnetic Properties of Ultrathin Ni/Fe Bilayers Grown Epitaxially on Ag(001)", Physics

Review B. 38, 12879, 1988.

[4.4] H. Sato, R. S. Toth, and R. W. Astrue, in "Single Crystal Films", Edited by M. H. Francombe and H. Sato (Pergamon, New York, 1964), pp.393 - 412.

# 5 List of Appendices

**Appendix 1**: Kerr Effect Data Processing Program

**Appendix 2**: Data Measurement Procedures

**Appendix 3**: Temperature Control Program

## Appendix 1

### Kerr Effect Data Processing Program

```
60 REM KEDP.ZQM. 06/22/88
70 CLS
80      PRINT      "************************************"
90 PRINT "   *  KERR EFFECT DATA PROCESSING          *"
100 PRINT "  *            PROGRAM  1.3                *"
110   PRINT   "          ************************************"
115 PRINT
120 PRINT " NOTE: THIS PROGRAM COLLECT DATA FROM"
130 PRINT " NICOLET AND RAW DATA ON DIVE A AS A "
135 PRINT  "FILE. IT ALSO CAN GENERATE"
140 PRINT " A GRAGH FILE FOR THE PROGRAM 'TELLAGRAF'"
145  PRINT  "IN MTS "
150 PRINT " INPUT TITLE AND THE X AXIS LABELED AS"
160 PRINT " 'GAUSS', THE Y AXIS LABELED AS 'KERR ROTATION'."
170 PRINT
180 PRINT
190 INOUT " DO YOU WANT MAKE A MEASUREMENT (M) OR
GENERATE A GRAGH FILE (G) (M OR G)?", G$
200 PRINT
210 DIM A!(1024)
220 DIM B!(1024)
320 IF G$="G" OR G$="g" THEN 1260
330 IF G$="M" OR G$="m" THEN 340 ELSE 280
```

```
340 PRINT
350 PRINT  " Connect address cable to DACO."
360 PRINT
370 PRINT  " Connect data cable to ADCO."
380 PRINT
390 PRINT
400 PRINT
410 PRINT "Press READOUT key on NICOLET before start this
program!"
420 PRINT
430 PRINT
440 INPUT  " Give a name (FILENAME.EXT) for your DATA FILE:",
NA$
450 PRINT
460 PRINT
470 INPUT  " Is this measurement ofr sample or magnetic
field(S or F)?", NN$
480 IF NN$="S" OR NN$="s" THEN 500
490 IF NN$="F" OR NN$="f" THEN 520 ELSE 470
500 OPEN "0", #1, "C:"+NA$
510 GOTO 620
520 OPEN "0", #2, "C:"+NA$
530 PRINT
540 PRINT  "Set the 'VOLTS FULL SCALE' at (+/-)2V on NICOLET
and"
550 PRINT  "Set the 'VERTICAL DISPLAY SCALE' at 512
MAGNITUDE/DIVISION."
```

```
560 PRINT
570 INPUT  "What 'FULL SCALE RANGE' on the GAUSS METTER?",
RANGE!
580 PRINT
590 PRINT  " Measure the field driven by the FUNCTION
GENERATOR for one time."
600 PRINT
610 PRINT
620 PRINT
630 PRINT
640 LET M=1024
650 INPUT  "Start collecting data now (Yor N)?", ANS$
660 IF ANS$="Y" OR ANS$="Y" THEN 670 ELSE GOTO 650
670 BEEP
680 BEEP
690 REM PROGRAM ADC CHANNEL 0. READ DATA FROM NICOLET.
700 FOR I=0 TO M-1
710 OUT 1812, 128
720 OUT 1813, 0
730 OUT 1814, 0
740 IF INP(1812)<128 THEN 740
750 LOW%-INP(1813)
760 HIGH%=INP(1814)
770 A!(I)=256*HIGH%+LOW%
780 IF A!(I)>32767 THEN A!(I)=A!(I)-65536!
790 IF NN$="F" OR NN$="f" THEN B!(I)=A!(I)
800 OUT 1841,179
```

```
810 OUT 1840,48
820 OUT 1841,128
830 OUT 1840,0
840 PRINT "Channel";I "=";A!(I)
850 NEXT I
860 IF NN$="F" OR NN$="f" THEN 1080
870 IF NN$="Y" OR NN$="y" THEN 1170
880 FOR I=0 TO 1023
890  PRINT #1,A!(I)
900 NEXT I
910 BEEP
920 BEEP
930 BEEP
940 PRINT
950 PRINT "The original data file already exists on drive C!!!"
960 PRINT
970 INPUT "An other measurement(Y or N)?",NNN$
980 IF NNN$="Y" OR NNN$="y" THEN 1060
990 IF NNN$="N" OR NNN$="n" THEN 1000 ELSE 960
1000 PRINT
1010 PRINT "If you finished the measurements of both Kerr
effect"
1020 PRINT  "and Magnetic field, do you want to create a graph
file"
1030 PRINT " for MTS TELLAGRAF program (Y or N)?",GAS$
1040 IF GAS$="Y" OR GAS$="y" THEN 1260
1050 IF GAS$="N" OR GAS$="n" THEN 1880 ELSE 1000
```

```
1060 CLS
1070 GOTO 340
1080 PRINT
1090 PRINT " NOW YOU SHOULD MEASURE THE ZERO FIELD READING"
1100 PRINT
1110 PRINT " COMPUTER ONLY COLLECT 100 DATA POINTS IN THIS CASE!"
1120 PRINT
1130 INPUT "START DATA COLLECTNG NOW(Y OR N)?",NN$
1140 IF NN$="Y" OR NN$="y" THEN 1150 ELSE 1130
1150 LET M=100
1160 GOTO 690
1170 LET Z!=0
1180 FOR I=5 TO 99
1190  Z!=Z!+A!(I)/95
1200 NEXT I
1210 FOR I=0 TO 1023
1220 B!(I) = (B!(I)-Z!)*RANGE!/226
1230 PRINT #2,B!(I)
1240 NEXT I
1250 GOTO 910
1260 PRINT
1270 INPUT "GIVE A NAME FOR THE GRAPH FILE(NAME.EXT):",GAN$
1280 PRINT
1290 CLOSE
```

```
1300 OPEN "O",#3,"C:"+GAN$
1310 INPUT "INPUT X AXIS FILENAME(NAME.EXT)?:",XF$
1320  PRINT
1330 INPUT "INPUT Y AXIS FILENAME(NAME.EXT)?:",YF$
1340  PRINT
1350 INPUT "INPUT GRAPH TITLE:?",TITLE$
1360 OPEN "I",#1,"C:"+XF$
1370 OPEN "I",#2, "C:"+YF$
1380 FOR J=1 TO 1024
1390  INPUT  #1,A!(J)
1400 NEXT J
1410 FOR J=1 TO 1024
1420  INPUT  #2,B!(J)
1430 NEXT J
1440  PRINT
1450 INPUT "DELETE SOME DATA POINTS(Y OR N)?",S$
1460 IF S$="Y" OR S$="y" THEN 1920
1470 IF S$="N" OR S$="n" THEN 1480 ELSE 1450
1480 LET N=0
1490 LET M=0
1500  PRINT
1510 INPUT "DO YOU WANT TO SMOTH THE DATA OF Y AXIS(Y OR
N)?",SM$
1520 IF SM$="Y" OR SM$="y" THEN 1540
1530 IF SM$="N" OR SM$="n" THEN 1710 ELSE 1500
1540  PRINT
1550 INPUT "SMOTH N TIMES, INPUT N=?",NT
```

```
1560 DIM C!(1024)
1570 FOR I=1 TO NT
1580 LET C!(N)=(69*B!(N)+4*(B!(N+1)+B!(N+3))-6*B!(N+2)-
B!(N+4))/70
1590 LET C!(N+1) = (2*B!(N)+ B!(N+4)) +27*B!(N+1) +12*B!(N+2)
-8*B!(N+3))/35
1600 FOR L=N+2 TO 1021-M
1610 LET C!(L) =(-3*(B!(L-2)+B!(L+2)) +12*(B!(L-1)+B!(L+1)) +
17*B!(L))/35
1620 NEXT L
1630 LET C!(1022-M)= (2*B!(1019-M)+ B!(1023-M)+ B!(1023-
M))-8*B!(1020-M) +12*B!(1021-M)-27*B!(1022-M))/35
1640 LET C!(1023-M)=(-B!(1019-M)+4*(B!(1020-M)+B!(1022-
M))-6*B!(1021-M)+69*B!(1023-M))/70
1650 FOR J=N TO 1023-M
1660 LET B!(J)=C!(J)
1670 NEXT J
1680 PRINT
1690 PRINT "SMOTH "I" TIMES!"
1700 NEXT I
1710 PRINT #3,"INPUT DATA."
1720 FOR J=N TO 1023-M
1730 PRINT #3,A!(J),B!(J)
1740 NEXT J
1750 PRINT #3,"END OF DATA."
1760 PRINT #3,"TITLE IS "TITLE$"."
1770 PRINT #3,X AXIS LABEL IS 'GAUSS'."
```

```
1780 PRINT #3,Y AXIS LABEL IS 'KERR EFFECT ROTATION'."
1790 PRINT #3,"BORDER OFF."
1800 PRINT #3,"FRAME THE PLOT."
1810 PRINT #3, "X GRID ON."
1820 PRINT #3,"Y GRID ON."
1830 PRINT #3, "X AXIS LENGTH IS 8."
1840 PRINT #3,"FRAME THE PLOT."
1850  LET  D=1024-N-M
1860  PRINT
1870  PRINT "THE GRAPH FILE HAS"D" DATA POINTS AND
ALREADY EXISTS ON DRICE C!!!"
1880 BEEP
1890 BEEP
1900  PRINT
1910 END
1920  PRINT
1930 INPUT "DELETE FIRST N POINTS, N=",N
1940  PRINT
1950 INPUT "DELETE LAST M POINTS, M=",M
1960  PRINT
1970 GOTO 1500
```

## Appendix 2

## DATA MEASUREMENT PROCEDURES

### 1. Setup NICOLET for Kerr effect measurement

(1) Use digital voltmeter to measure the photodiode output signal level and set the "Volts Full Scale" at a proper range (± 1/4 V ).

(2) INPUT FILTER = 50

(3) Choose "VIEW INPUT".

(4) SYSTEM NOISE REDUCTION = ON.

(5) RESOLUTION = 12 bits.

(6) "SUB" OR "ADD" both OK, but don't change it during the measurement.

(7) Adjust the "DC LEVEL", set the signal to the center of the screen.

(8) CONTINUOUS DISPLAY = OFF.

(9) PEN = REAL TIME.

(10) SWEEP RETURN = FLAYBACK.

(11) TRIGGER = "+".

(12) Adjust "DELAY" and "DWELL TIME" to meet the period of the function generator. Don't change it during the measurement.

(13) HORIZONTAL DISPLAY SCALE = NORMAL.

(14) MEMORY ADDRESS GROUP = FULL for 1024 points setup.

(15) DATA TRANSFER DONER = FULL for 1024 points setup.

## 2. Transfer Data From NICOLET to Computer

(1) Push "STOP" key.

(2) Set READOUT PROGRAM = PEN.

(3) DWELL TIME = 1x EXT ADDR ADV.

(4) Push "READOUT" key.

(5) Start "KEDP.ZQM" program on the computer. follow the instructions displayed on the screen.

## 3. Magnetic Field Measurement

(1) Don't change the setup of the NICOLET in the Kerr signal measurement.

(2) AUTO STOP = "1"

(3) VERTICAL DISPLAY SCALE = 512.

(4) VOLTS FULL SCALE = ± 2 V.

(5) Adjust the DC LEVEL let the scan spot at the center of the screen for zero field.

(6) Push MEASURE to measure the field for one period.

## 4. Transfer Field Data to Computer

(1) Set the NICOLET back to the transfer mode.

(2) Repeat the transfer procedures for Kerr data transfer.

## 5. Transfer Graph File From PC to MTS.

C:> MTS (RETURN)

#R *KERMIT (RETURN)

>SERVER (RETURN)

ZSTEM? K (RETURN)

SEND (RETURN)

A: FILENAME.EXT (RETURN)

## Appendix 3

## Temperature Control Program

```
30 CLS
40    PRINT    "**************************************"
50 PRINT "*      Temperature Control Program          *"
60    PRINT    "**************************************"
100 PRINT "                    ZHONG QINGMING"
130 PRINT "    This program can control the temperature in the"
140 PRINT " range of -200 to 0 centigrade degree. The uncertainty is"
150 PRINT " ± 0.7 centigrade degree."
160 PRINT " Connecte DAC-01 to the heater power supply. ConnectE"
170 PRINT " ADC-0 to thermocouple readout. For the amplifier,"
180 PRINT " Zi = 10E4, Ci = 10E-8, Zf = 10E7, Cf = 10E-9."
190 PRINT
240 DIM A!(201)
250 OPEN "I" ,#1, "\KERR\TABL2"
260 FOR I=0 TO 200
270 INPUT #1, X, A!(I)
280 NEXT I
290 REM SEND 0 VOLTS TO THE HEATER.
300 OUT 1811,0
310 OUT 1810,7
```

```
320 PRINT
330 INPUT "WHAT TEMPERATURE DO YOU WANT?", N
340 IF N>=-200 AND N<=0 THEN 400
350 PRINT
360 PRINT "THE NUMBER IS OUT OFF RANGE. TRY AGAIN."
370 PRINT
380 PRINT
390 GOTO 330
400 CLS
410 LOCATE 5,9
420 PRINT "TEMPERATURE EXPECTED",N,"HEATER"
430 LOCATE 7,9
440 PRINT "TEMEPRATURE MEASURE T."
450 LOCATE 24,9
460 PRINT "PRESS ANY KEY TO SET A NEW TEMPERATURE."
470 REM READ TEMPERATURE T.
480 OUT 1812,128
490 OUT 1813,0
500 OUT 1814,0
510 A$=INKEY$:IF A$=" " THEN 300
520 IF INP(1812)<128 THEN 520
530 LOW%=INP(1813)
540 HIGH%=INP(1814)
550 T!=256*HIGH%+LOW%
560 IF T!>32767 THEN T!=T!-65536!
570 IF T!==>A!(0) AND T!=<A!(200) THEN 610
580 PRINT
```

```
590 PRINT "TEMPERATURE MEASURED OUT OFF RANGE!"
600 GOTO 400
610 IF T!-A!(-N)<0 THEN 810
620 FOR M=0 TO 200+N-1
630 IF A!(-N+M+1)=>T! AND T!=>A!(-N+M) THEN 660
640 NEXT M
650 GOTO 480
660 LOCATE 4,65
670 PRINT "ON!"
680 LOCATE 6,43
690 LET HT!=N-M-(T!-A!(-N+M)/(A!(-N+M+1)-A!(-N+M))
700 PRINT USING "+###.#";HT!
710 REM SEND 10 VOLTS TO THE HEATER.
720 IF M>25 THEN 780
740 LET NN=INT((T!-A!(-N))*200
750 IF NN>128 THEN 780
760 OUT 1811,0
770 GOTO 480
780 OUT 1811,1
790 OUT 1810, 128
800 GOTO 480
810 FOR M=0 TO -N-1
820 IF A!(-N-M)=>T! AND T!=>A!(-N-M-1) THEN 850
830 NEXT M
840 GOTO 480
850 LOCATE 4,65
860 PRINT "OFF!"
```

```
870 LOCATE 6,43
880 PRINT USING "+###.#"; N+M+(A!(-N-M)-T!)/(A!(-N-M)-A!(-
M-N-1))
890 REM SEND 0 VOLTS TO THE HEATER
900 OUT 1811,0
910 OUT 1810,7
920 GOTO 480
930 END
```